Entropy-driven population distributions in a prototypical molecule with two flexible side chains: *O*-(2-acetamidoethyl)-*N*-acetyltyramine

V. Alvin Shubert, Esteban E. Baquero, Jasper R. Clarkson,[a] William H. James III, Jeffrey A. Turk,[b] Alissa A. Hare,[c] Kevin Worrel, and Mark A. Lipton
Department of Chemistry, Purdue University, West Lafayette, Indiana 47907-2084, USA

Daniel P. Schofield and Kenneth D. Jordan
Department of Chemistry, University of Pittsburgh, Pittsburgh, Pennsylvania 15260, USA

Timothy S. Zwier[d]
Department of Chemistry, Purdue University, West Lafayette, Indiana 47907-2084, USA

(Received 6 August 2007; accepted 4 October 2007; published online 20 December 2007)

Resonant two-photon ionization (R2PI), resonant ion-dip infrared (RIDIR), and UV-UV hole-burning spectroscopies have been employed to obtain conformation-specific infrared and ultraviolet spectra under supersonic expansion conditions for *O*-(2-acetamidoethyl)-*N*-acetyltyramine (OANAT), a doubly substituted aromatic in which amide-containing alkyl and alkoxy side chains are located in *para* positions on a phenyl ring. For comparison, three single-chain analogs were also studied: (i) *N*-phenethyl-acetamide (NPEA), (ii) *N*-(*p*-methoxyphenethyl-acetamide) (NMPEA), and (iii) *N*-(2-phenoxyethyl)-acetamide (NPOEA). Six conformations of OANAT have been resolved, with S_0-S_1 origins ranging from 34 536 to 35 711 cm^{-1}, denoted $A-F$, respectively. RIDIR spectra show that conformers $A-C$ each possess an intense, broadened amide NH stretch fundamental shifted below 3400 cm^{-1}, indicative of the presence of an interchain H bond, while conformers $D-F$ have both amide NH stretch fundamentals in the 3480–3495 cm^{-1} region, consistent with independent-chain structures with two free NH groups. NPEA has a single conformer with S_0-S_1 origin at 37 618 cm^{-1}. NMPEA has three conformers, two that dominate the R2P1 spectrum, with origin transitions between 35 580 and 35 632 cm^{-1}. Four conformations, one dominate and three minor, of NPOEA have been resolved with origins between 35 654 and 36 423 cm^{-1}. To aid the making of conformational assignments, the geometries of low-lying structures of all four molecules have been optimized and the associated harmonic vibrational frequencies calculated using density functional theory (DFT) and RIMP2 methods. The S_0-S_1 adiabatic excitation energies have been calculated using the RICC2 method and vertical excitation energies using single-point time-dependent DFT. The sensitivity of the S_0-S_1 energy separation in OANAT and NPOEA primarily arises from different orientations of the chain attached to the phenoxy group. Using the results of the single-chain analogs, tentative assignments have been made for the observed conformers of OANAT. The RIMP2 calculations predict that interchain H-bonded conformers of OANAT are 25–30 kJ/mol more stable than the extended-chain structures. However, the free energies of the interchain H-bonded and extended structures calculated at the preexpansion temperature (450 K) differ by less than 10 kJ/mol, and the number of extended structures far outweighs the number of H-bonded conformers. This entropy-driven effect explains the presence of the independent-chain conformers in the expansion, and cautions future studies that rely solely on relative energies of conformers in considering possible assignments. © *2007 American Institute of Physics*. [DOI: 10.1063/1.2803076]

I. INTRODUCTION

The field of molecular spectroscopy has increasingly focused attention on molecules of sufficient size and flexibility to possess many conformational isomers. One of the fruitful strategies used to study these molecules is to incorporate into the molecule an ultraviolet chromophore that can be readily detected using either laser-induced fluorescence or resonant two-photon ionization.[1–12] By cooling the molecules in a supersonic expansion, ultraviolet transitions due to single conformers can often be resolved. Double resonance schemes can then be employed to determine the number of conformational isomers present and to map out the ultraviolet and infrared spectral signatures of individual conformers.

Spectroscopic data of this type provide important testing grounds for force field and electronic structure methods. From the standpoint of theory, one of the most useful and direct points of comparison with experiment would be the

[a]Present address: Eastman Chemical Company, Kingsport, TN 37662.
[b]Present address: Department of Chemistry, Alma College, Alma, MI 48801.
[c]Present address: Department of Chemistry, Yale University, New Haven, CT 06520-8107.
[d]Author to whom correspondence should be addressed. Electronic mail: zwier@purdue.edu

relative energies of the minima. Unfortunately, spectroscopic measurements, in general, do not directly yield relative energies. In cases where the conformational population is in thermal equilibrium, relative intensities can be used to extract energy differences from the Boltzmann factor. However, many of the molecules currently under study are large enough that supersonic expansion cooling is needed to resolve the transitions due to individual isomers. This situation has ignited an ongoing debate about the degree to which the observed intensities in jet-cooled spectra reflect the preexpansion thermal equilibrium population, or are modified by the cooling that occurs during expansion.[11,13–24]

In a few cases, this foundation of conformation-specific spectroscopy has served as the basis for population transfer studies that directly measure the energy thresholds to isomerization between pairs of conformers. When the isomerization threshold is measured for both the $X \rightarrow Y$ and $Y \rightarrow X$ directions, this places constraints on the relative energies of the zero-point levels of the two minima, $\Delta E = E_Y - E_X$.[25–29] However, the vast majority of experimental studies deduce the relative energies of the conformers (or at least the energy ordering) based on the relative intensities of the observed transitions.

The preponderance of studies in this field have been directed at molecules with biological relevance, leading to impressive progress in the spectroscopy of amino acids,[3,5,6,9,30,31] DNA bases,[32–40] and small polypeptides.[3,31,41–50] The present study has a somewhat different focus and goal. Here we synthesize and study the single-conformation spectroscopy of a molecule, *O*-(2-acetamidoethyl)-*N*-acetyltyramine [OANAT, Scheme 1(a)], more for the anticipated topology of its potential energy surface than for its direct biological relevance. OANAT possesses two methyl-capped, amide-containing flexible side chains, anchored in *para* positions to a phenyl ring via flexible alkyl or alkoxy connectors.

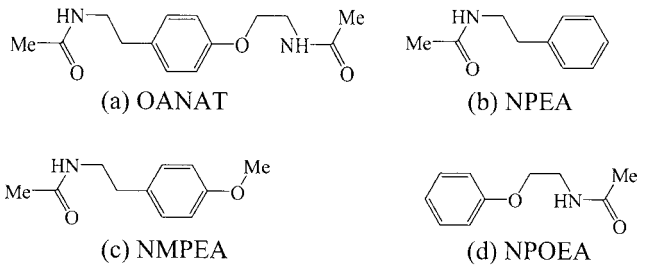

Scheme 1

By incorporating two independent side chains that point in opposite directions from the phenyl ring that separates them, much of the potential energy landscape for OANAT ought to be dictated by the preferences and properties of the individual side chains. To explore this possibility, conformation-specific spectroscopy has also been carried out on the corresponding single-chain molecules: *N*-phenethyl-amide [NPEA, alkyl chain only, Scheme 1(b)] and *N*-(2-phenoxyethyl)-acetamide [NPOEA, alkoxy chain only, Scheme 1(d)]. A simple double-chain analog, *N*-(*p*-methoxyphenethyl-acetamide) [NMPEA, Scheme 1(c)], is also considered to probe the initial effects of a second independent side chain (the methoxy group) on the spectroscopy.

A striking consequence of incorporating both chains into the same molecule is the large increase in the complexity of the potential energy surface that results. If n conformational minima are present in one chain and m in the other, one might expect $n \times m$ conformers for the double-chain molecule. However, this estimate ignores the fact that the chains break the symmetry of the aromatic ring that connects them, producing up to four distinct double-chain conformers for each (i,j) chain conformer pair (pointing up or down, to the right or left). It also ignores the possibility that the chains could interact, either directly (e.g., via an interchain hydrogen bond) or indirectly through the aromatic ring, introducing new conformational minima.

A powerful visualization of the increased complexity of the OANAT potential energy surface relative to that of its single-chain analogs is provided by examining the associated disconnectivity diagrams, which graphically display the energies of the local minima and their connectivity through isomerization barriers.[51] Constructing a full disconnectivity diagram requires locating all local minima and transition states on the potential energy surface and establishing the minimum energy pathways between the minima and transition states. Their calculation for molecules of the size of OANAT would be extraordinarily challenging for high level *ab initio* theory, but can be accomplished using classical force fields. Figure 1 presents the disconnectivity diagrams for NMPEA, NPOEA, and OANAT obtained using the general AMBER force field (GAFF).[52] The production of these diagrams is described in detail in Sec. IV. As anticipated, the disconnectivity diagram for the double-chain OANAT is far more complicated than its single-chain counterparts. In particular, with the GAFF we have located 10 minima for NPEA (disconnectivity diagram not shown), 18 for NMPEA, 26 for NPOEA, and 893 for OANAT.

The disconnectivity diagrams of all four molecules divide into major branches containing structures with amide groups that have adopted *trans* or *cis* configurations. These branches are separated by large barriers, 60–80 kJ/mol, typical of *trans-cis* secondary amide isomerization,[53–55] creating two main branches in the disconnectivity diagrams of NPEA, NMPEA, and NPOEA, and four branches for OANAT. Not surprisingly, most of the low-energy structures have the amide group(s) in the *trans* configuration. For OANAT, many of these low-lying structures incorporate conformations in which the two chains are not interacting, but adopting extended configurations found in NPEA and NPOEA. However, the low-lying *trans/trans* (and *cis/trans*) structures of OANAT include a subset in which an interchain H bond is formed by folding the two chains back over the ring to form an amide-amide H bond.

In this paper we present conformation-specific infrared (IR) and ultraviolet (UV) spectra of NPEA, NMPEA, NPOEA, and OANAT. Transitions due to one, three, four, and six conformers are observed for NPEA, NMPEA, NPOEA, and OANAT, respectively. A tentative but self-consistent set of assignments is made for these conformers

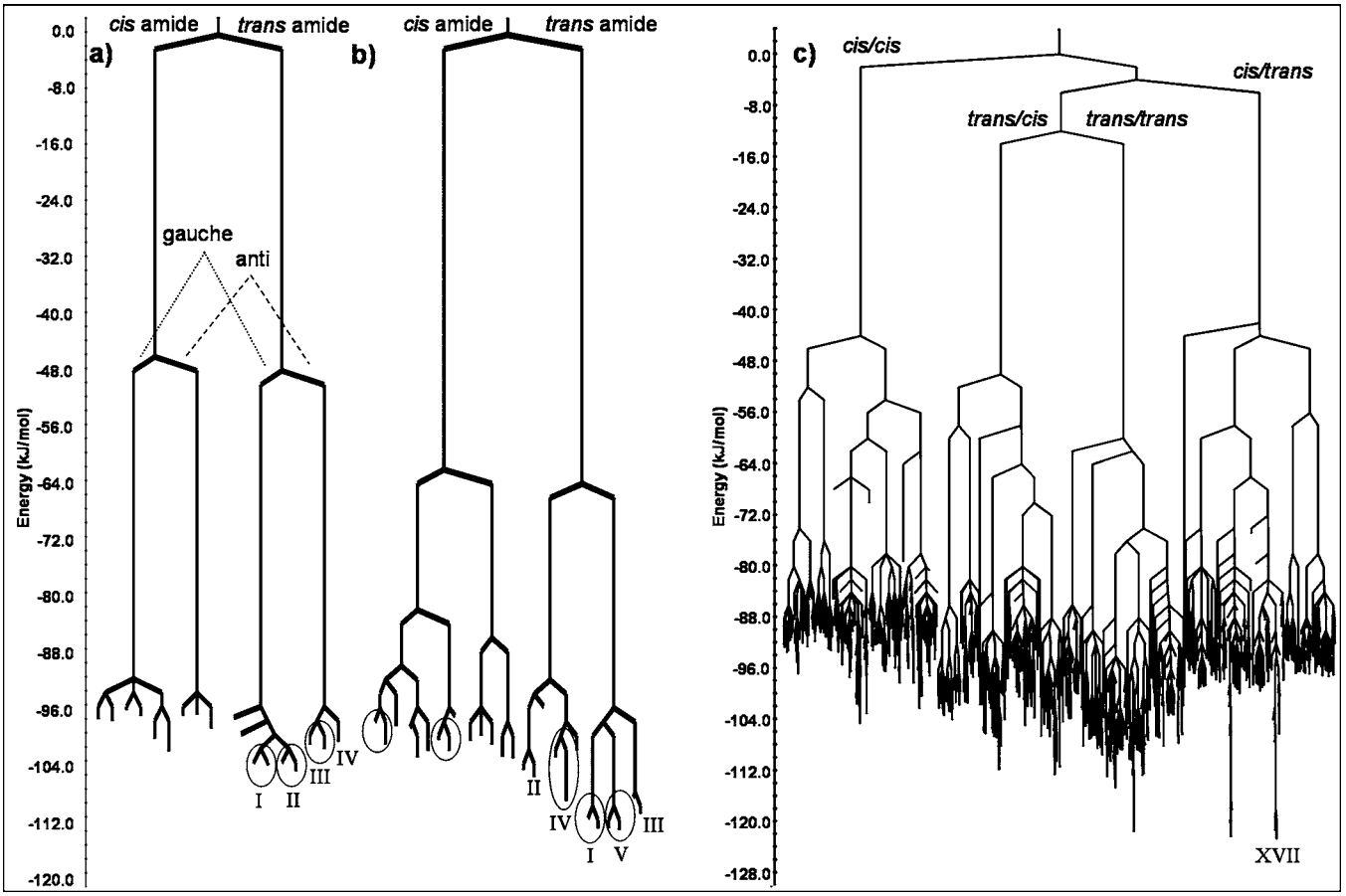

FIG. 1. Disconnectivity diagrams for (a) NMPEA, (b) NPOEA, and (c) OANAT using the general AMBER force field (GAFF). Roman numerals label structures on which higher level calculations were performed. Pairs of structures that optimized to the same geometry at the RIMP2 level of theory are circled. Labels for *trans/trans* amide structures of OANAT have been omitted for clarity. Absolute energies from GAFF have been shifted by 80.0, 34.0, and 224.0 kJ/mol for NMPEA, NPOEA, and OANAT, respectively, placing the first node connecting all minima at 0.0 kJ/mol.

based on several pieces of spectroscopic data. Each amide group provides a pair of infrared spectroscopic handles, the NH and CO stretches, that can serve as diagnostics for structural determination of individual conformations. The analogous spectra in the alkyl CH stretch region also show patterns that support division of the observed conformers into subgroups.[56] Finally, the ultraviolet spectra also hold clues to the conformation, based on large variations in the S_0-S_1 origin transition frequencies and the extent and type of low-frequency vibronic structure observed.

The structures, relative energies, harmonic vibrational frequencies, and (where possible) S_0-S_1 transition energies for many of the low-lying conformational minima of NPEA, NMPEA, NPOEA, and OANAT have been characterized using electronic structure methods, providing several points of comparison between theory and experiment. These calculations predict that for OANAT some of the interchain H-bonded conformers are 20–30 kJ/mol lower in energy than any of the noninteracting chain structures. As we shall see, the energetic preference for interchain H-bonded conformers is counterbalanced by an opposing entropic term favoring population of the independent-chain conformers, leading to the observation of both types of conformers experimentally.

II. EXPERIMENTAL METHODS

The molecular beam time-of-flight mass spectrometer used for the resonant two-photon ionization (R2PI) experiments consists of two differentially pumped vacuum chambers, shown in Fig. 2, built around a commercial ion source and time-of-flight tube (R. M. Jordan). Turbomolecular pumps, Pfeifer TMH 1001 and Pfeifer TMH 261, each backed by a mechanical pump (Sargent 1397), were used to evacuate the source chamber and detection chambers, respectively. Typical operating pressures under gas load for source and detection chambers were 1×10^{-5} and 1×10^{-6} mbar, respectively.

Details of the synthesis of NMPEA, NPOEA, and OANAT are presented in the supplementary material.[56] NPEA was used as supplied (Fisher Scientific, 98% purity). The molecules of interest were heated (heater rope, Varian) in the sample holder, positioned immediately behind the pulsed valve (Parker General Valve, Series 9, 0.8 mm orifice, 20 Hz). Temperatures of approximately 115, 130, 130, and 180 °C for NPEA, NMPEA, NPOEA, and OANAT, respectively, were used. The buffer gas, a 70% neon/30% helium mixture (Spectra Gases), was held at a backing pressure of 2–2.5 bar.

Electronic spectra were recorded by employing one-color R2PI. The frequency-doubled output of neodymium-

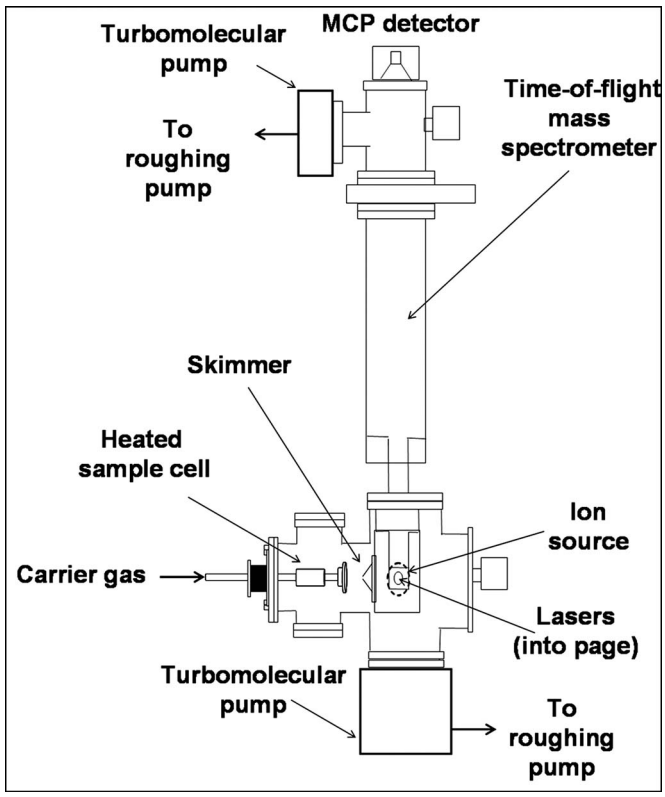

FIG. 2. Schematic of the time-of-flight mass spectrometer used in this work. The lasers are propagated perpendicular to the molecular beam.

doped yttrium aluminum garnet (Nd:YAG) (Continuum) pumped tunable dye lasers (Lambda-Physik Scanmate, Lumonics Hyperdye) was used as ultraviolet sources. Ion signals were amplified [25×, Stanford Research System (SRS) model SR445] then sent to a gated integrator (SRS model SR250). Monomer ion signals and integrator gate position were monitored by using a digital oscilloscope (Agilent 54642A). Laser control and data collection were accomplished through a personal computer employing a suite of LABVIEW programs [National Instruments (NI), version 5.0] and data acquisition cards (NI).

The electronic spectra of specific conformations were recorded using UV-UV hole-burning. A higher power hole-burning laser (10 Hz) was fixed on a transition in the R2PI spectrum and the probe laser (20 Hz) was scanned over the wavelength region of interest. In Sec. V, asterisks are placed in the figures on the transitions used for hole-burning, which were the S_0-S_1 origins in all cases except NPEA and NMPEA(*C*). The hole-burning and probe lasers were counterpropagated, spatially overlapped, and separated temporally so the hole-burning laser preceded the probe by 200 ns. The hole-burning spectra were recorded by monitoring, via active baseline subtraction, the difference between the ion signal due to the probe laser with the hole-burning laser "on" or "off." All bands that originate from the same ground state level as the transition on which the hole-burn laser is fixed appear as depletions in the ion signal.

Conformation-specific IR spectra were obtained using resonant ion-dip infrared (RIDIR) spectroscopy.[57,58] A seeded Nd:YAG pumped parametric converter (LaserVision, KTA based, 10 Hz) produced tunable infrared radiation from 2800 to 3600 cm^{-1} with typical powers of 1–5 mJ/pulse. The IR and probe UV lasers were counterpropagated, spatially overlapped, and temporally separated so the IR laser preceded the probe by 200 ns. The probe laser wavelengths were fixed on the same transitions in the electronic spectra used for UV-UV hole-burning and the ion signal monitored while the IR was tuned. IR transitions arising from the same ground state level as the probe laser resonance produce depletions in the ion signal. As in UV-UV hole-burning, active baseline subtraction was employed to compare the difference between IR laser on or off. The tuning range of the IR system used in this experiment was expanded to include the region 1000–1900 cm^{-1} by using a $AgGaSe_2$ crystal, described previously.[59]

III. THE CONFORMATIONAL PREFERENCES OF RELATED SINGLE-CHAIN MOLECULES

Before taking up our experimental and computational results, we consider first what is known about the conformational preferences of analogous alkyl and alkoxy-substituted benzenes from previous work. If the known conformational preferences of smaller alkyl and alkoxy-substituted benzenes establish a pattern that carries over as the chains are expanded in length, they can assist spectral interpretation and assignments for NPEA, NMPEA, NPOEA, and OANAT.

The ethyl group is the shortest possible flexible alkyl side chain. Under supersonic jet-cooled expansion conditions, ethylbenzene exists as a single conformer.[60] The carbon bonded to the aromatic ring (C_X) remains in the plane of the ring while the second carbon in the chain (C_Y) is out of plane such that the dihedral angle $\tau(C_{ortho(C)}-C_{ipso(C)}-C_X-C_Y) \approx 90°$ (see Scheme 2, which has atom types as defined by Bernstein *et al.*[61]).[60] This conformation, with the C_X-C_Y bond perpendicular to the ring, both minimizes steric repulsion and allows hyperconjugation between the C_X-C_Y σ bond of the chain and aromatic π system.[60]

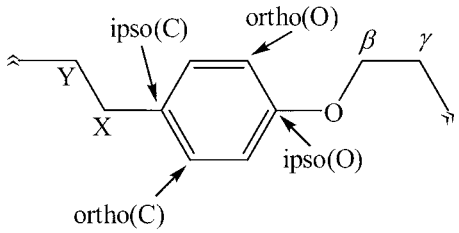

Scheme 2

Studies of the longer alkyl chains in phenethylamine[62–65] (PEA), tyramine,[63] and *p*-methoxyphenethylamine[10,12,63,66,67] (MPEA) demonstrate that the conformational preferences established in ethylbenzene are retained in the homologous series of longer chains; i.e., $\tau(C_{ortho(C)}-C_{ipso(C)}-C_X-C_Y) \approx 90°$ in all observed chains in which the first two atoms are carbon atoms. In addition, a feature common to alkyl-amine chains is a preference for gauche conformers which are stabilized through a $NH\cdots\pi$ interaction with the ring.[30,62–65]

These preferences also extend to alkyl chains attached to other aromatic rings such as indole in tryptamine,[9,68] 3-indole-propionic acid,[69] and tryptophan.[70]

The conformational preferences are changed when the flexible side chain involves oxygen as a linker group between the phenyl ring and side chain. Previous studies have identified a single conformational isomer for methoxybenzene, for which both heavy atoms remain in the plane of the ring, giving $\tau(C_{ortho(O)}-C_{ipso(O)}-O-C_\beta)\approx 0°$ or 180°.[71] This structure is stabilized by conjugation between the lone pair electrons in the oxygen *p*-type orbital and the aromatic π system that dominates over repulsive steric forces.[61] Ethoxybenzene also has a single origin at 36 372 cm^{-1} that has been assigned to a planar anti structure with $OC_\beta C_\gamma$ in plane and the terminal methyl group anti to the ring.[61] Two conformers of 2-phenoxyethylamine (POEA, $C_6H_5-OCH_2CH_2NH_2$) have been detected and assigned, with S_0-S_1 origins at 36 367 and 36 382 cm^{-1}.[7] Both conformers were assigned as anti-gauche, denoted as *AGx*, where *A* and *G* denote the anti or gauche configuration of the $C_{ipso(O)}-O-C_\beta-C_\gamma$ and $O-C_\beta-C_\gamma-N$ atom chains, respectively, and the lower case *x* describes the $C_\beta-C_\gamma-N$-lone pair chain as either anti *a* or gauche *g*.[7]

In what follows, we will use the same nomenclature used by Macleod and Simons[7] to describe the alkoxy chain conformations present in NPOEA and OANAT, but using the lower case *x* to describe the orientation of the $C_\beta-C_\gamma-N-C$ dihedral. As in NPEA and NMPEA, pairs of structures that differ only in orientation of the amine lone pair collapse to a single structure upon substitution of the acetyl group onto the amine.

Given the preferred in-plane conformation for alkoxy chains, it initially seemed unlikely to us that the two chains in OANAT would be able to directly interact, since to do so would require the alkoxy chain to bend back over the ring, disturbing the in-plane preference. However, as we shall see shortly, this energy cost can be compensated by stabilization gained from interchain interactions in the form of amide-amide H bonds.

IV. THEORETICAL METHODS

For molecules with a large number of torsional degrees of freedom, it is not tractable to locate all the low-energy minima by scanning the dihedral angles. Even for a moderately sized molecule such as OANAT, such an approach would be computationally prohibitive, especially if used in conjunction with *ab initio* electronic structure methods. In this work we have adopted the strategy of using a force field method for doing an initial characterization of the stationary points (i.e., minima and first-order saddle points) of OANAT and its single-chain analogs. The low-energy minima located using the force field approach were then used to initiate geometry optimizations with the Becke3LYP density functional method[72,73] with an *ultrafine* grid and *tight* optimization criteria. The resulting minima were then reoptimized with the resolution of the identity second-order Möller-Plesset perturbation theory (RIMP2) method,[74–76] which gives energies comparable to those from traditional MP2 calculations, but requires a factor of 5–10 less computer time for the molecules considered here.

The all atom GAFF, with atomic charges obtained from the semiempirical AM1 bond charge correction approach, was used to survey the potential energy surfaces (PES).[52] Local minima on the PES of each molecule were found using the basin-hopping algorithm[77] which uses Monte Carlo moves on a transformed landscape, with the transformation being accomplished via limited memory Broyden-Fletcher-Goldfarb-Shanno[78] (LBFGS) optimizations to local minima after each Monte Carlo move. At each Monte Carlo step the torsional angles were varied by random amounts between −90° and 90°. The temperatures of the simulations were adjusted to give acceptance ratios of 0.5. For NPEA, POEA, and NMPEA, 4 runs of 1000 Monte Carlo steps were performed, and for OANAT 15 runs of 3000 steps were performed. The basin-hopping runs were performed with the GMIN2.0 program of Wales and co-workers.[79]

For each minimum found in the basin-hopping runs, the Hessian was calculated using GAFF and a search for transition states initiated by walking uphill in both directions along the ten modes with the smallest eigenvalues using the eigenvector following method.[80,81] Upon location of a transition state, the minima it connects were identified by stepping using LBFGS minimizations (in both directions) off the transition state along the eigenvector corresponding to the imaginary eigenvalue. When this approach located a previously unknown local minimum, it was added to the database of minima. The minima, transition states, and pathway information were then combined to assemble the disconnectivity diagrams shown in Fig. 1. The transition state searches and path following calculations were performed with the OPTIM3.2 program.[79]

As mentioned previously, the low-energy minima located with the strategy described above were reoptimized using the B3LYP density functional method[72,73] with the 6-311+G(*d*) basis set.[82] The resulting B3LYP minima were then reoptimized using the RIMP2 method[74–76] with the aug-cc-pVDZ′ basis set, which consists of the aug-cc-pVDZ basis set on the heavy atoms and the cc-pVDZ basis set on the H atoms.[83–88] For selected conformers the calculations were repeated with the full aug-cc-pVDZ basis set on all atoms, and the resulting relative energies were found to be very close to those from the aug-cc-pVDZ′ basis set, thereby justifying use of the mixed basis set. Harmonic vibrational frequencies were calculated at the B3LYP/6-311+G(*d*) level for all four molecules considered and at the RIMP2/aug-cc-pVDZ′ level for NPEA, NMPEA, and NPOEA.

As a further aid in the conformational assignments of NPEA, NMPEA, and NPOEA, vertical excitation energies to the S_1 state were obtained from resolution of the identity approximate coupled clusters singles and doubles (RICC2) method[89] with the aug-cc-pVDZ′ basis set and RIMP2 optimized geometries. For selected conformers (due to high computation cost), the S_1 excited states were optimized using the RICC2 method, providing estimates of the adiabatic excitation energies. Single-point time-dependent density func-

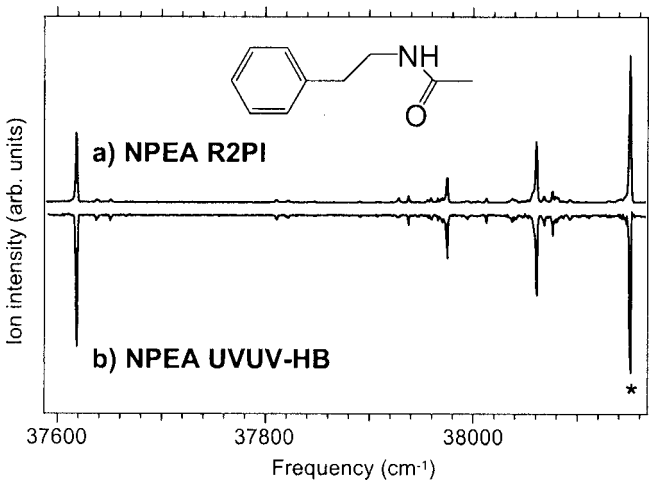

FIG. 3. (a) The R2P1 excitation spectrum of NPEA taken over the region near the S_0-S_1 origin. (b) UV-UV hole-burning spectrum taken with the hole-burn laser fixed as indicated with an asterisk.

tional theory (TDDFT) B3LYP calculations were performed on all of the molecules, providing a point of comparison where RICC2 excitation energies were unavailable. The B3LYP calculations were carried out with the GAUSSIAN 03 suite of programs,[90] and the RIMP2 and RICC2 calculations were performed with TURBOMOLE.[91]

V. RESULTS AND ANALYSIS

A. NPEA

The R2PI and UV-UV hole-burning spectra, obtained with the hole-burn laser fixed at 38 150 cm^{-1}, of NPEA are shown in Fig. 3. All transitions observed in the R2PI spectrum are accounted for in the hole-burning spectrum, proving that a single conformation is responsible for all of them. The most intense band in the excitation spectrum occurs at 532 cm^{-1} above the origin and is assigned to the $6a_0^1$ ring fundamental characteristic of substituted benzenes.[92,93] The hole-burning spectrum is somewhat more saturated than the R2PI spectrum, accounting for the observed differences in intensities between the two.

A conformational search with GAFF found a total of ten local minima for NPEA, but at the RIMP2 level these collapse to eight distinct local minima, three of which are *trans*-amide structures. The relative energies of these three conformers are summarized in Table I. The extra minima from GAFF (e.g., the two minima that collapse to structure I) are associated with rotations of the terminal methyl group. The RIMP2 conformers can be classified as anti or gauche, depending on the position of the amide group relative to the phenyl ring. The RIMP2 optimized structures (see supplementary material)[56] for the lowest-energy anti and gauche conformational minima of NPEA share an out-of-plane orientation for the ethylacetamide side chain.

The electronic origin of the single observed conformer of NPEA, 37 618 cm^{-1}, is in the same region as an analogous molecule, phenethylamine (PEA, $C_6H_5CH_2CH_2NH_2$), which has four origins between 37 538 and 37 629 cm^{-1}. These four conformers have been assigned as pairs of anti and gauche structures differing in the orientation of the amino group, with gauche conformers dominating the spectrum.[62,63] In NPEA the substitution of the acetyl group forms a planar amide subunit, collapsing the pair of anti structures in PEA into a single anti conformer in NPEA. Similarly, the three orientations of the amino group in PEA reduce to a single gauche conformer in NPEA.

Based on its close similarity with PEA, it is natural to assign the single observed transition in NPEA to the gauche conformation NPEA-I. The observed low-frequency vibronic transitions (Table II) at 18 and 32 cm^{-1} are consistent with this assignment with B3LYP/6-311+G(*d*) frequencies of 21 and 34 cm^{-1} for the two lowest torsional modes of the gauche conformer (NPEA-I) and frequencies of 30 and 38 cm^{-1} for the anti conformer (NPEA-II).[94] This assignment is also in keeping with the calculated relative energies for the two conformers, in particular, with the RIMP2 calculations that place the gauche structure 8.4 kJ/mol lower in energy and 4.6 kJ/mol lower in free energy than the anti structure (Table I).

B. NMPEA

Figure 4 reports the R2PI and UV-UV hole-burning spectra of NMPEA, which differs from NPEA by substitution of a methoxy group para to the ethylacetamide side chain. The hole-burning spectra reveal the presence of three conformers, of which the two denoted *A* and *B* dominate and a third, denoted *C*, is several times weaker in intensity.

The GAFF calculations predicted 18 local minima for NMPEA that, at the RIMP2 level, collapse to 15 minima. Seven pairs of structures in NMPEA have ethylacetamide side chain conformers identical to those in NPEA, differing in orientation of the methoxy group (*cis* or *trans*) relative to the long chain. The remaining conformer is a *cis* amide anti structure with the amide plane perpendicular to the ring plane, so that a 180° rotation of the $O-CH_3$ bond produces an equivalent structure. Figure 5 represents the four lowest-energy conformers of NMPEA optimized at the RIMP2 level of theory. All four of these conformers have a *trans* amide configuration and calculations predict an energetic preference of gauche over anti conformers, as was found for NPEA. This result is also in keeping with the experimental findings on MPEA, whose ultraviolet spectrum was dominated by transitions due to gauche ethylamine conformations.[10]

The ultraviolet spectra of conformers *A* and *B* of NMPEA are of similar intensity and more intense than *C*, have S_0-S_1 origins differing by only 9 cm^{-1}, and the associated hole-burning spectra display nearly identical low-frequency vibronic structure. Figure 6(a) presents the infrared spectra in the NH stretch region of the NMPEA conformers. The most striking feature of the spectra is the 13 cm^{-1} decrease in frequency of *A* and *B* (both at 3482 cm^{-1}) relative to *C* (3495 cm^{-1}). This frequency shift is expected for gauche relative to anti conformers since the NH hydrogen of gauche conformers is involved in a weak π-hydrogen bond with the phenyl ring. Additionally, the NH stretch of NPEA occurred

TABLE I. Observed and calculated, S_0-S_1 origins, relative energies and free energies of NPEA, NMPEA, NPOEA, and OANAT.

Molecule	Isomer (assignment)	Expt. origin (cm^{-1})	T_c (cm^{-1})		ΔE (kJ/mol)[a]			Free energy correction (kJ/mol)[e]	ΔG (kJ/mol)[f]
			TDDFT[b]	RICC2[c]	B3LYP	RIMP2	B2-PLYP[d]		
NPEA	I (obs.)	37 618	42 557	39 261	0.0	0.0	⋯	0.0	0.0
	II	n/a	42 557	⋯	0.6	8.4	⋯	−3.8	4.6
	III	n/a	42 615	⋯	6.4	4.0	⋯	0.3	4.3
NMPEA	I (B)	35 589	39 540	36 097	0.0	0.0	⋯	0.0	0.0
	II (A)	35 580	39 465	36 077	0.3	0.5	⋯	−0.2	0.3
	III (C)	35 632	39 584	36 458	0.6	8.1	⋯	−3.4	4.7
	IV	n/a	39 634	36 535	1.0	8.5	⋯	−3.3	5.3
NPOEA	I (A)	36 423	40 791	37 401	0.0	0.0	⋯	0.0	0.0
	II	n/a	40 745	37 475	7.0	8.2	⋯	−0.3	8
	III (C)	36 127	40 327	36 987	8.8	3.4	⋯	−1.7	1.7
	IV (B)	36 353	40 553	37 361	10.0	3.0	⋯	4.6	7.6
	V[g] (D)	35 656	40 072	35 996	10.9	−7.8	⋯	8.4	0.6
OANAT	I (E)	35 622	39 654	36 029	0.0	28.0	15.5	−21.0	7.0
	II		39 640	35 969	0.0	27.5	15.2	−21.0	6.5
	III (D)	35 608	39 601	35 945	0.2	28.0	15.3	−20.8	7.2
	IV		39 595		0.3	27.9	15.4	−20.3	7.6
	V		39 712		0.2	36.1	17.8	−20.0	16.2
	VI (F)	35 711	39 708		0.3	35.8	17.8	−19.9	15.9
	VII		39 758		0.1	35.7	17.3	−20.5	15.3
	VIII		39 755		0.1	35.7	17.2	−20.2	15.5
	IX		38 947		10.5	17.2	16.3	−20.1	−2.9
	X (A)	34 536	38 183	34 083	9.4	0.0	0.0	0.0	0.0
	XI (B)	34 539	38 830		17.0	7.2	8.2	−0.4	6.8
	XII (C)	35 549	39 694		21.2	11.0	10.6	−3.5	7.5
	XIII		39 577	36 109	11.8	2.6	3.9	−1.2	1.4
	XIV		40 389		18.2	21.8	17.6	−7.5	14.3
	XV		39 412		20.8	10.5	11.5	−3.9	6.6
	XVI		39 687		13.5	6.9	5.9	−2.3	4.6
	XVII		38 827		18.0	17.6	12.6	1.0	18.6

[a]Energies include vibrational zero-point corrections calculated with unscaled frequencies from the same level of theory as the geometry optimizations [B3LYP/6-311+G(*d*) or RIMP2/aug-cc-pVDZ′] except OANAT for which B3LYP frequencies were used.
[b]Single-point time-dependent density functional theory, B3LYP/6-311+G(*d*), on B3LYP optimized structures.
[c]Adiabatic electronic excitation energies at RICC2/aug-cc-pVDZ′ from RIMP2/aug-cc-pVDZ′ optimized geometries.
[d]B2-PLYP/aug-cc-pVDZ′.
[e]Gibbs corrections calculated at preexpansion sample temperatures using unscaled RIMP2 frequencies and geometries except for OANAT for which B3LYP values were used.
[f]ΔG=free energy correction+ΔE(RIMP2).
[g]B3LYP and RIMP2 optimizations gave rise to significantly different NPOEA-V structures (see Fig. 8).

at 3484 cm^{-1} (see supplemental material),[56] very close to the frequency observed for NMPEA *A* and *B*. These features support the assignment of NMPEA(*A*) and NMPEA(*B*) to gauche structures that differ in the methoxy orientation, *cis* or *trans*, and NMPEA(*C*) to an anti conformation. Furthermore, comparison with MPEA where gauche-*trans* and gauche-*cis* structures occur in pairs, with gauche-*trans* conformer origins appearing red of gauche-*cis*,[10] suggests an assignment of *A* to the gauche-*trans* structure, NMPEA-II, and *B* to the gauche-*cis* structure, NMPEA-I. As confirming evidence, the RICC2 calculations predict a redshift of the adiabatic excitation energy of the S_0-S_1 transition of NMPEA-II from NMPEA-I (Table I).

The position of the S_0-S_1 origin of *C* (35 632 cm^{-1}), shifted blue of *A* and *B*, is consistent with its assignment as an anti conformation. However, two anti conformers, differing in orientation of the methoxy group, were anticipated and it is possible that transition *C* has contributions from both NMPEA-III and NMPEA-IV. Since the amide group of an anti conformer interacts weakly with the ring, it is plausible that these two conformers will have similar S_0-S_1 origin frequencies.

The B3LYP frequency calculations are consistent with the structural assignments, predicting the NH stretch frequencies to be nearly the same in the two gauche conformers and to lower frequency than the NH stretch of the anti conformer. However, the calculated shifts are on the order of 3 cm^{-1}, while the observed shifts are on the order of 10 cm^{-1}. The RIMP2 calculations also predict nearly identical NH stretch frequencies for the gauche structures but place these 30 cm^{-1} below the anti conformers. Thus, neither the B3LYP/6-311+G(*d*) nor the RIMP2/aug-cc-pVDZ′

TABLE II. Summary of relevant vibrational frequencies of NPEA, NMPEA, and NPOEA.

Molecule		Torsional modes (cm^{-1})[a] ν_1 Obs.	ν_1 B3LYP	ν_1 RIMP2	ν_2 Obs.	ν_2 B3LYP	ν_2 RIMP2	NH stretches (cm^{-1})[b] ν_{NH} Obs.	ν_{NH} B3LYP	ν_{NH} RIMP2
NPEA	I (A)	18	21	23	32	34	51	3484	3484	3484
	II	···	30		···	38		···	3487	3513
	III	···	16		···	21		···	3479	3469
NMPEA	I (B)	22	17	20	33	31	46	3482	3483	3481
	II (A)	22	19	19	35	28	47	3482	3482	3482
	III (C)	31	29	28	47	33	35	3495	3486	3512
	IV	···	27	29	···	33	31	···	3486	3513
NPOEA	I (A)	20	16	23	···	34	39	3491	3491	3491
	II	···	28	30	···	33	38	···	3491	3511
	III (C)	···	13	10	25[c]	28	38	3491	3488	3488
	IV (B)	···	36	40	···	42	45	3499	3493	3508
	V (D)	32	18	42	57[c]	32	58	3488	3494	3478

[a]Unscaled.
[b]B3LYP and RIMP2 NH stretch frequencies of NPEA and NMPEA are scaled by 0.9585 and 0.9603, respectively, to bring the calculated frequency of NPEA-I into agreement with experiment. B3LYP and RIMP2 NH stretch frequencies are scaled by 0.9586 and 0.9575, respectively, to bring the calculated frequency of NPOEA-I into agreement with the measured frequency of NPOEA-(*A*).
[c]From vibronic bands observed in the hole-burning spectra.

calculations predict the correct magnitude for the NH stretch frequency difference between anti and gauche structures in this class of molecules.

Further support for the assignments is found by examining the low-frequency torsional modes that give rise to the vibronic structure observed in both the hole-burning and single vibronic-level fluorescence (SVLF) spectra, provided in the supplementary material.[56]

Table II summarizes the observed and calculated torsional frequencies, together with the assignments. As seen from Table II, the B3LYP/6-311+G(*d*) frequencies are consistent with the assignment of *A* to NMPEA-II, *B* to NMPEA-I, and *C* to an anti structure (III or IV). For the most part, RIMP2 calculations give low-frequency modes similar to those obtained from the B3LYP calculations, with the exception of the second lowest-frequency mode of NMPEA-I and NMPEA-II, which, like the corresponding mode of NPEA, has an appreciably higher frequency in the RIMP2 calculations.

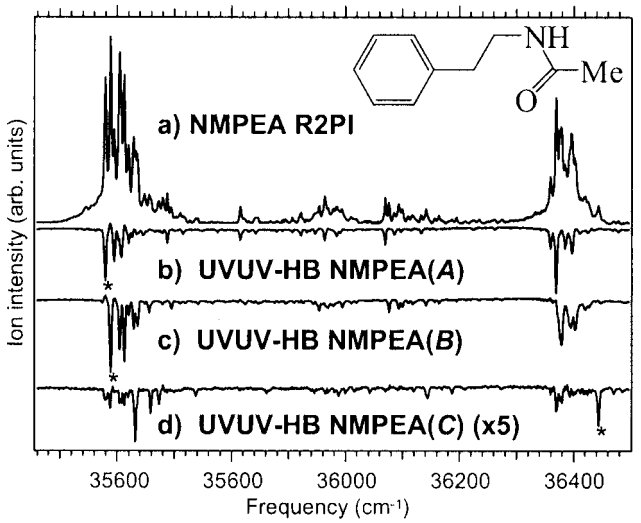

FIG. 4. (a) R2P1 excitation spectrum of NMPEA taken over the region near the S_0-S_1 origins. [(b)–(d)] UV-UV hole-burning spectra taken with the hole-burn laser fixed as indicated by the asterisks.

C. NPOEA

The electronic and UV-UV hole-burning spectra for NPOEA are shown in Fig. 7. A single conformer (*A*) dominates the electronic spectrum, but contributions from three minor conformers (*B*–*D*) are also observed, with intensities 20–50 times weaker than conformer *A*. This large intensity

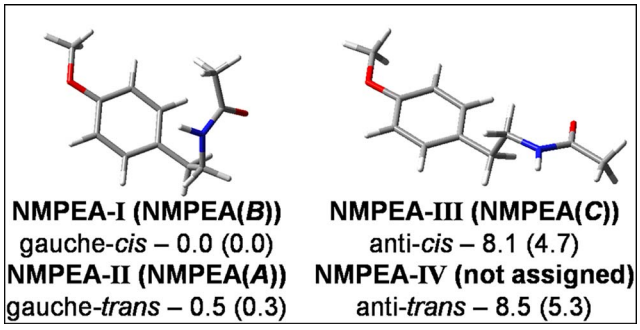

FIG. 5. (Color online) The lowest-energy structures, with *cis* orientation of methoxy group pictured, of NMPEA from RIMP2 optimizations. Relative vibrational zero-point corrected energies (kJ/mol) are reported with the relative free energies in parentheses. The *trans* orientation of the methoxy group is produced by 180° rotation of $C_{ortho(O)}-C_{ipso(O)}-O-C_\beta$ dihedral.

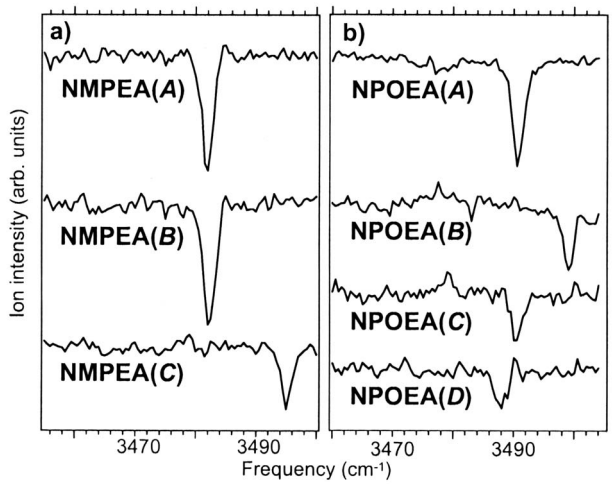

FIG. 6. RIDIR spectra in the amide NH stretch region of (a) NMPEA and (b) NPOEA.

difference suggests a strong energetic preference for a single conformation of the oxyethylacetamide chain.

The basin-hopping calculations with the GAFF give 26 minima for NPOEA. As seen from the disconnectivity diagram in Fig. 1, these divide into *cis* and *trans* amide branches separated by a barrier of about 90 kJ/mol. Upon optimization with the RIMP2 method, the 12 conformers on the *trans* amide branch collapse to 9 distinct minima. Figure 8 presents the five most stable conformational isomers of NPOEA optimized at the RIMP2 level. Of these five structures, I–IV have extended chains and V^b has the chain folded back over the ring.

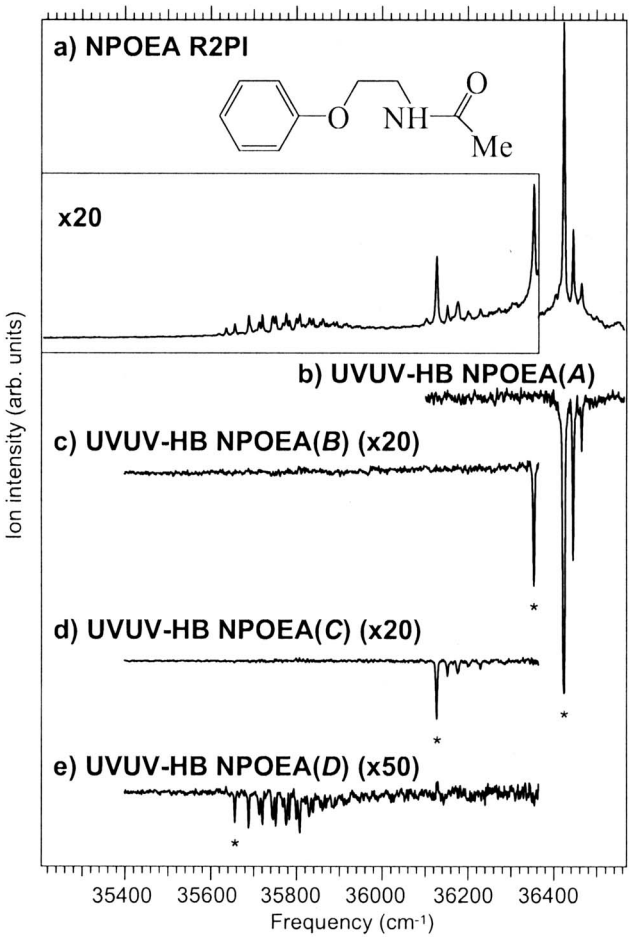

FIG. 7. (a) R2P1 excitation spectrum of NPOEA taken over the region near the S_0-S_1 origins. [(b)–(e)] UV-UV hole-burning spectra taken with hole-burn laser fixed on the transitions marked by asterisks.

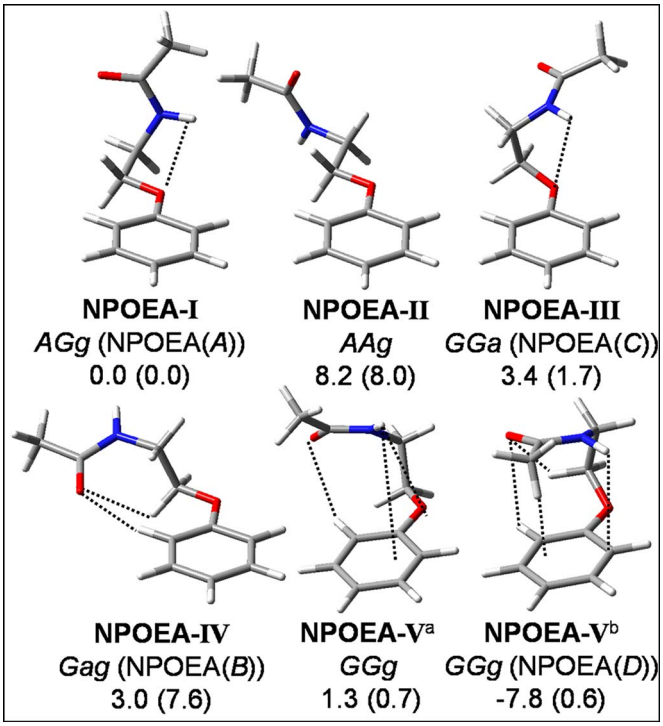

FIG. 8. (Color online) The five lowest-energy RIMP2 optimized NPOEA structures and one (NPOEA-V^a) from B3LYP optimization. Relative vibrational zero-point corrected (ZPC) energies (kJ/mol) are reported along with relative free energies in parentheses. ZPC relative and free energies of NPOEA-V^a were obtained from single-point MP2/6-311+G(*d*) and B3LYP frequency calculations on the B3LYP geometry. Dashed lines indicate potentially stabilizing interactions.

NPOEA-I shares the same *AGg* conformation as the two observed conformers of POEA.[7] It thereby retains the expected preference for an in-plane orientation for the C_β and C_γ carbons first noted for smaller alkoxy chains.[7,61,71] This structure is also the global minimum at the B3LYP/6-311+G(*d*) level of theory. The relative energies of the five conformers are appreciably altered upon optimization at the RIMP2/aug-cc-pVDZ′ level of theory, most notably in reversing the energy ordering of NPOEA-I and NPOEA-V^b, predicting that the latter is 7.8 kJ/mol more stable than the former. Given the bias of the MP2 method for folded structures (e.g., the benzene dimer π-stacked system[95]), we have also performed single-point CCSD(T)/aug-cc-pVDZ calculations [as implemented in MOLPRO (Refs. 96 and 97)] on the RIMP2/aug-cc-pVDZ′ optimized geometries. Indeed, the CCSD(T) calculations predict NPOEA-I and NPOEA-V^b to be nearly isoenergetic. Unlike conformers I–IV, for NPOEA-V the RIMP2 and B3LYP methods give very different structures (Fig. 8). The RIMP2 structure has the side chain positioned directly over the ring with which it interacts strongly through both the terminal methyl group and the amide NH. The large structural difference between the B3LYP and RIMP2 optimized structures for this conformer

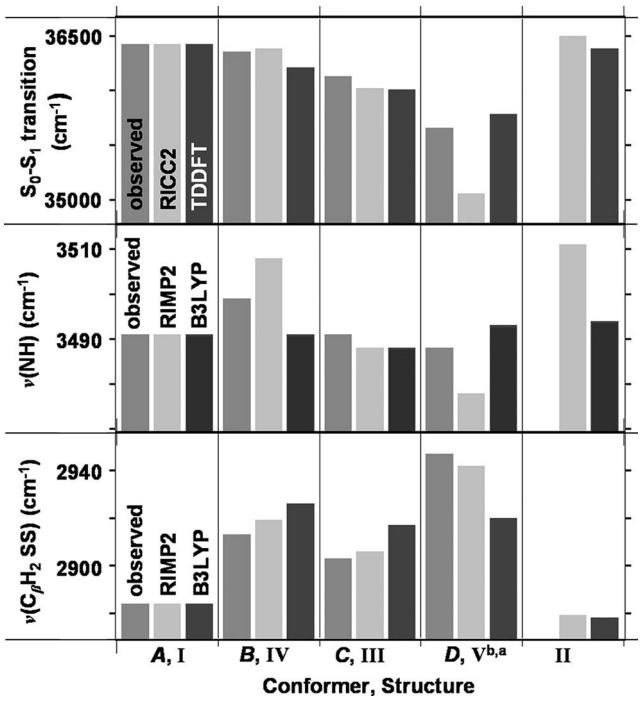

FIG. 9. Evidence used for assigning the observed conformers of NPOEA. Letters denote the observed conformers and Roman numerals indicate calculated data for the structures shown in Fig. 8. The theoretical results are scaled to match NPOEA-I to NPOEA(*A*), with the RICC2 and TDDFT S_0-S_1 values scaled by 0.9244 and 0.8929, respectively. Vibrational frequencies are scaled by factors given in Table II and Fig. 10.

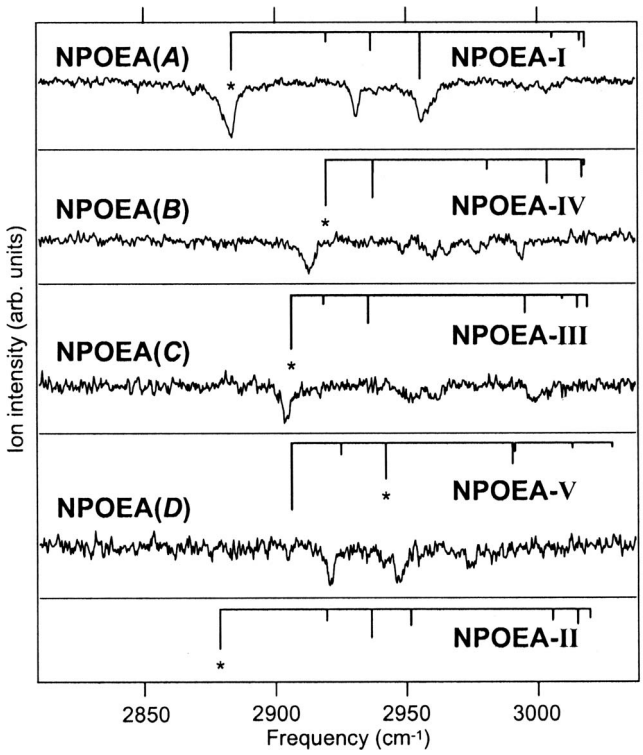

FIG. 10. RIDIR spectra of NPOEA in the alkyl CH stretch region. RIMP2 alkyl CH stretch frequencies (scaled by 0.9467) and IR intensities are presented above the conformer to which they are assigned, with NPOEA-II included at the bottom. The $C_\beta H_2$ symmetric methylene stretch fundamentals are indicated with asterisks on the calculated spectra.

is a consequence of long-range dispersion interactions that are underestimated by the B3LYP calculations.[98,99]

Conformational assignments for the four conformers of NPOEA are made based on combined evidence from the conformation-specific UV and IR spectra. These data lead to assignments of NPOEA(*A*) to NPOEA-I, NPOEA(*B*) to NPOEA-IV, NPOEA(*C*) to NPOEA-III, and NPOEA(*D*) to NPOEA-V^b. Figure 9 summarizes the key experimental data that support these assignments.

An important trend uncovered from examination of the RIMP2 vibrational frequencies of NPOEA is illustrated in the stick spectra in the alkyl CH stretch region included in Fig. 10. The symmetric methylene stretch of the $C_\beta H_2$ groups, marked by asterisks in the figure, is diagnostic of the local conformation of the alkoxy group. In structures with C_γ out of plane (structures III–V^b) the $C_\beta H_2$ symmetric stretch is shifted to higher frequency than those conformers in which C_γ remains in plane (structures I and II). The observed alkyl CH stretch spectra of NPOEA presented in Fig. 10 show distinct differences in the symmetric CH stretch region that track the calculations. Based on their comparison, the NPOEA conformers can be classified into families of structures, with NPOEA(*A*) having C_γ in plane and NPOEA(*B–D*) having C_γ out of plane. This trend was also observed in the B3LYP calculations, although the predicted shifts were less pronounced.

The most distinguishing spectroscopic feature of the conformers of NPOEA is the positions of the S_0-S_1 origins, spread over almost 800 cm^{-1} (Table I), in contrast to NMPEA where all three S_0-S_1 origins occurred within 52 cm^{-1} of one another. This result indicates that the oxygen atom that links the phenyl ring to the ethylacetamide chain plays an active role in modulating the S_0-S_1 energy separation. A second distinguishing feature of the hole-burning spectra in Fig. 7 is the extent and intensity of the observed low-frequency vibronic structure, which involves torsional motions of the flexible side chain. Conformers *A–C* display short vibronic progressions (Table II), and the weak intensity of this structure indicates a small change in geometry between ground and excited states. By contrast, conformer *D* has extensive low-frequency progressions that extend more than 200 cm^{-1} above the S_0-S_1 origin. The larger geometry change associated with conformer *D* must result from a side chain conformation that interacts strongly with the π cloud of the aromatic ring that is responsible for the electronic transition.

Building upon the classification of the NPOEA conformers as having C_γ in plane [NPOEA(*A*)] or out of plane [NPOEA(*B–D*)], the trends in S_0-S_1 origins and vibronic activity make more definitive assignments possible. NPOEA-I and NPOEA-II have geometries with both C_γ and C_β in plane. Accompanying this geometry are the largest computed S_0-S_1 energy separations. These observations, together with the strong energetic preference of NPOEA-I over NPOEA-II at both the B3LYP and RIMP2 levels of theory, argue for the assignment of NPOEA(*A*) to NPOEA-I. This assignment is consistent with the observed origin transition frequencies and the lack of significant low-frequency vibronic activity observed in ethoxybenzene[64] and POEA.[7]

The remaining conformers $B-D$ must then have C_γ and/or C_β out of plane to some degree, consistent with assignments to structures NPOEA-III–V, with NPOEA-II not observed in our experiment. Conformer D, with its large electronic redshift (-762 cm^{-1}) from A (Table I, Fig. 9) and intense low-frequency vibronic activity, is most consistent with NPOEA-V^b. Its folded structure promotes strong interaction between the side chain and ring, consistent with the observed vibronic structure. This conformer is also the only one of the five that has a large redshift (-1400 cm^{-1} relative to NPOEA-I) in its calculated S_0-S_1 energy separation.

Of the two remaining RIMP2 optimized structures (III and IV), NPOEA-III has the largest computed S_0-S_1 frequency shift (-414 cm^{-1} at RICC2) from NPOEA-I, suggesting assignment of NPOEA-III to NPOEA(C) for which the observed shift of the S_0-S_1 band relative to that of NPOEA(A) of -297 cm^{-1}. Although NPOEA-III has C_γ out of plane, it contains a chain-ring interaction similar to NPOEA-I, in keeping with the similar Franck-Condon activity evident for NPOEA(C) and NPOEA(A). NPOEA(B), with the least redshifted origin from NPOEA(A), is assigned as NPOEA-IV, consistent with the smallest computed redshift in S_0-S_1 transition from NPOEA-I.

Confirming evidence for the assignments is provided by the RIDIR spectra in the NH stretch region, which are included in Fig. 6(b).[100] Table II lists the frequencies of the amide NH stretch fundamentals measured for conformers $A-D$, and calculated for conformers I–V^{a,b} at the B3LYP and RIMP2 levels of theory. Once again, the proposed structural assignments have the trends in the calculated frequencies of the amide NH stretch vibrations consistent with experiment (Fig. 9). The calculated shifts are smaller than experiment with B3LYP, and larger than experiment with RIMP2, the same behavior noted previously for NMPEA, with the RIMP2 results more in keeping with our intuition based on the structural interactions present.

The NH stretch of NPOEA(A) and C occurs at the same frequency, 3491 cm^{-1}, evidence that the NH group is in a similar environment in these two conformers, consistent with the proposed assignments of A to NPOEA-I and C to NPOEA-III. Both I and II configure the side chain so as to allow the formation of a weak H bond between the NH group and linking oxygen. NPOEA(B) has the highest-frequency NH stretch, 3499 cm^{-1}, indicating that the NH hydrogen is not involved in any intramolecular interactions, again consistent with the assignment of NPOEA(B) as NPOEA-IV. NPOEA(D) has the lowest-frequency NH stretch fundamental (3488 cm^{-1}), evidence that the NH hydrogen is participating in a stronger intramolecular interaction than in the other conformers. NPOEA-V^b, assigned to conformer D above, fulfills this criterion, with the side chain folded back over the ring in such a way that the NH group interacts strongly with the π cloud.

The assignments for the four conformers of NPOEA (A to I, B to IV, C to III, and D to V) were made with minimal reference to the calculated relative electronic energies for the conformers. This situation arose in part because of the sensitivity of the relative energies to the level of theory, particularly the RIMP2 prediction that NPOEA-V^b is 7.8 kJ/mol more stable than NPOEA-I, while CCSD(T) calculations predict the two structures to be nearly isoenergetic. Furthermore, the downstream populations may not be dictated by relative energies alone, but may instead reflect the preexpansion thermal equilibrium populations, which are determined by the relative free energies at the source temperature (400 K). In order to test the magnitude of this effect, we calculated free energy corrections for NPOEA-I–V^b using the RIMP2 structures and vibrational frequencies. These corrections favor NPOEA-I, with its extended and floppier structure, by 8.4 kJ/mol relative to NPOEA-V^b.

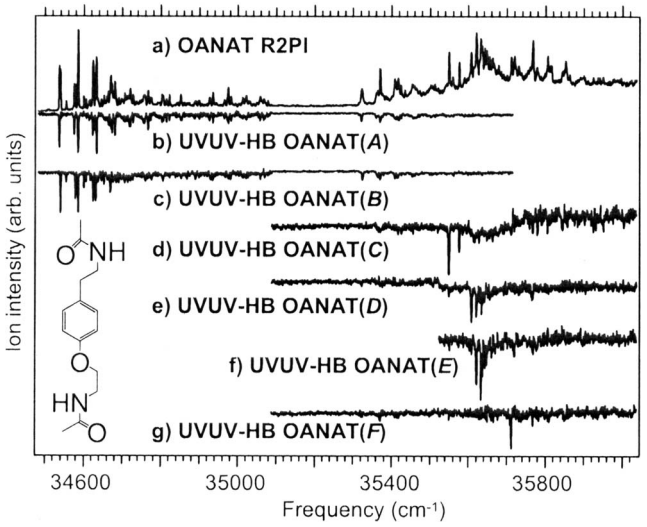

FIG. 11. Overview of R2PI and UV-UV hole-burning spectra of OANAT.

The high intensities of transitions due to NPOEA(A) (Fig. 7) compared to the other conformers of NPOEA suggest strongly that NPOEA(A) is significantly more populated than the other conformers. All spectroscopic evidence points to the assignment of NPOEA(A) to NPOEA-I and NPOEA(D) to NPOEA-V. These assignments are supported by free energy corrections that predict NPOEA-I to support a larger equilibrium population prior to expansion, which would be reflected in the expansion-cooled populations if the barriers to isomerization are sufficiently large that the equilibrium populations are largely retained during the expansion cooling process.

D. OANAT

Armed with the assignments on the single-chain analogs, we now turn attention to OANAT, the double-chain molecule that is the ultimate target of the present study. Figure 11 presents an overview of the R2PI and UV-UV hole-burning spectra of OANAT, and Fig. 12 presents a closeup of the hole-burning spectra around the origin transitions. Six origin transitions were resolved at 34 536, 34 539, 35 549, 35 608, 35 632, and 35 711 cm^{-1} for conformers labeled A, B, C, D, E, and F, respectively. As in NPOEA, the origins are spread over a wide frequency region, with the origins for A and B occurring over 1000 cm^{-1} to the red of those for the other four. Conformers A and B also have long Franck-Condon

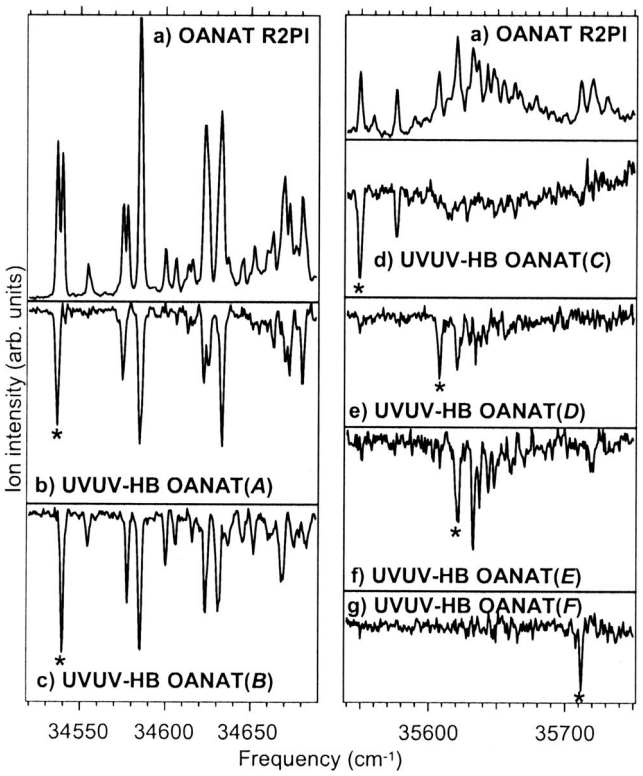

FIG. 12. Closeup of the S_0-S_1 origin regions of the six conformers of OANAT. The UV-UV hole-burning spectra were obtained by fixing the hole-burn laser on the transitions marked with asterisks.

progressions in their electronic excitation spectra, suggesting that as in NPOEA(D) there is significant interaction between the ring and side chain. Conformer F shows very little vibronic activity, indicating weak or negligible interactions of the side chains with the ring, similar to NPOEA(B) and C.

The NH stretch RIDIR spectra of OANAT are shown in Fig. 13, and the frequencies are listed in Table III. In addition

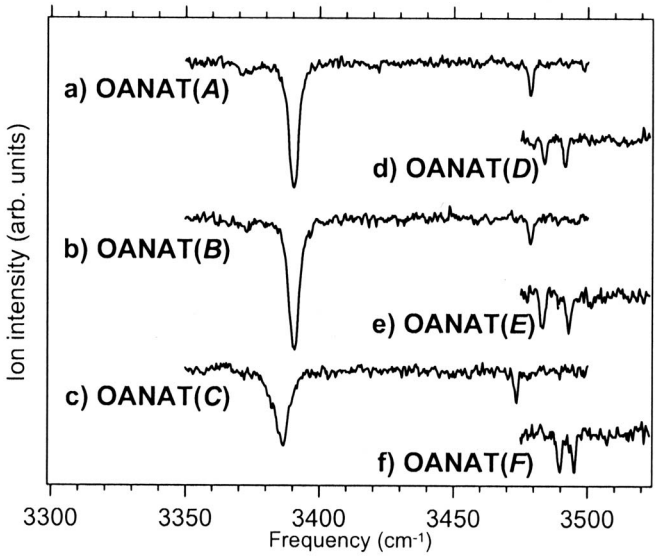

FIG. 13. [(a)–(f)] RIDIR spectra in the NH stretch region of the six conformers of OANAT.

to the "free" amide NH stretch fundamentals in the 3470–80 cm^{-1} region, conformers $A-C$ have NH stretch fundamentals that are shifted to lower frequency by more than 80 cm^{-1} from the other observed NH stretch frequencies. These NH stretch bands, at 3390 cm^{-1} for A and B and 3386 cm^{-1} for C, are also much more intense and broadened than typical NH stretches, characteristic signatures of a NH group involved in an intramolecular H bond. We conclude, therefore, that conformers $A-C$ of OANAT possess interchain H bonds. Conformers $D-F$ display two NH stretch fundamentals in the 3480–3500 cm^{-1} frequency range that is typical of those seen in the single-chain molecules, indicating that the chains are not interacting in these conformers.

The calculations using the GAFF located 893 minima for OANAT. The lowest-energy minima lie in the *trans/trans* and *cis/trans* funnels, where the labels indicate the conformations of the amide group on the alkoxy and alkyl chains, respectively. Whereas one would have expected all the low-lying local minima to reside in the *trans/trans* funnel, with GAFF there are seven minima in the *cis/trans* funnel that are within 5 kJ/mol of the global minimum. We note further than the lowest-lying local minima in both main funnels correspond to folded structures with interacting chains. B3LYP and RIMP2 optimizations were carried out on 16 low-lying minima in the *trans/trans* funnel as well as on the lowest-energy (according to GAFF) minimum in the *cis/trans* funnel. The resulting RIMP2 optimized structures are depicted in Figs. 14 and 15, from which it is seen that conformers I–IX are independent-chain structures and that X–XVII are folded structures containing interchain H bonds.

In the remainder of this paper we focus our attention on minima in the *trans/trans* funnel even though at the RIMP2 level of theory some of the considered extended structures in this funnel lie energetically above the examined folded structure in the *cis/trans* funnel. The major justification for this course of action is that there is no experimental evidence for the presence of *cis*-amide conformers, which would have sharp amide NH stretch fundamentals around 3420–3440 cm^{-1}.[101] Also, the GAFF global minimum *cis/trans* structure (OANAT-XVII, Fig. 15) contains an interchain H bond with the *trans* amide NH donating to the *cis* amide oxygen, producing two NH stretch fundamentals shifted to lower frequency, inconsistent with the observed spectra. Although the GAFF calculations predict OANAT-XVII as the global minimum, it is predicted to be 17.7 kJ/mol less stable than the global minimum in the *trans/trans* funnel at the RIMP2 level of theory. We shall also see shortly that XVII is further destabilized relative to the low-lying minima in the *trans/trans* funnel upon inclusion of entropy corrections (Table I).

E. Noninteracting side-chain conformers

In what follows, we assume that the preferred independent-chain structures of OANAT have conformations of the individual chains that are analogous to those found in the low-energy conformers of the single-chain analogs NPEA and NPOEA and the simpler double-chain model NMPEA. This is borne out by an analysis of the GAFF

TABLE III. Summary of the relevant vibrational frequencies of OANAT.

	Torsional modes (cm^{-1})[a]				ν_{NH} (cm^{-1})			
	ν_1		ν_2		Alkyl chain[b]		Alkoxy chain[c]	
Structure	Expt.	B3LYP	Expt.	B3LYP	Obs.	B3LYP	Obs.	B3LYP
I	(E) 11	11	15	15	3483	3484	3493	3491
II		10		18		3484		3492
III	(D) 13	12	16	13	3483	3485	3491	3491
IV		12		17		3485		3492
V	(F)	12	⋯	18	3495	3487	3490	3491
VI		12		22		3487		3491
VII		12		15		3487		3491
VIII		12		18		3487		3491
XI	⋯	12		18		3484		3495
X	(A)	24	38	36	3479	3479	3390	3411
XI	(B) 15	28	38	39	3479	3480	3390	3399
XII	(C) 27	21	⋯	33	3386	3382	3475	3477
XIII		23		31		3411		3477
XIV	⋯	17	⋯	24	⋯	3447	⋯	3487
XV	⋯	17	⋯	27	⋯	3479	⋯	3428
XVI	⋯	21	⋯	34	⋯	3419	⋯	3477
XVII	⋯	22	⋯	36	⋯	3409	⋯	3435

[a]Experimental values from vibronic progressions observed in the hole-burning spectra. Calculated frequencies are unscaled.
[b]Scaled by 0.9585, the scaling factor determined for NPEA.
[c]Scaled by 0.9586, the scaling factor determined for NPOEA.

minima, which have noninteracting chain conformers which, in large measure, can be readily assigned in this way.

The hole-burn spectra of conformers $D-F$ of OANAT are very similar in absolute frequency and vibronic structure to the three observed conformers of NMPEA($A-C$). NMPEA(A) and B have closely spaced origins assigned to gauche-*cis* and gauche-*trans* conformations, while NMPEA(C), assigned to an anti conformation of the alkyl chain, has an origin blueshifted from A and B. In OANAT, conformers D and E have S_0-S_1 origins at 35 608 and 35 622 cm^{-1}, respectively, differing by only 14 cm^{-1}, and a third conformer (F) at 35 711 cm^{-1}, shifted to the blue by 103 cm^{-1} from OANAT(E). OANAT(D) and E also mirror NMPEA(A) and B in their low-frequency vibronic structure.

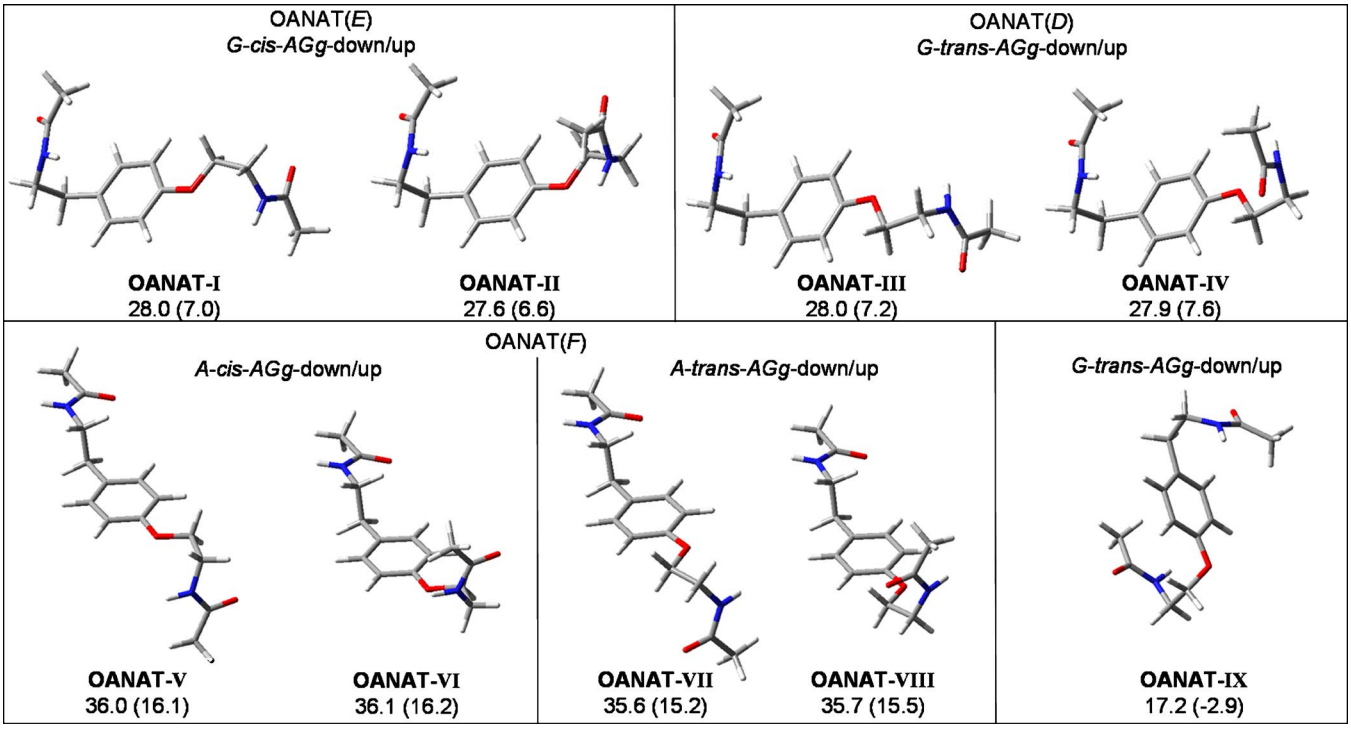

FIG. 14. (Color online) Lowest-energy noninteracting side chain conformers of OANAT. RIMP2/aug-cc-pVDZ′ energies (kJ/mol), vibrational zero point corrected using B3LYP frequencies, are given along with free energies in parentheses.

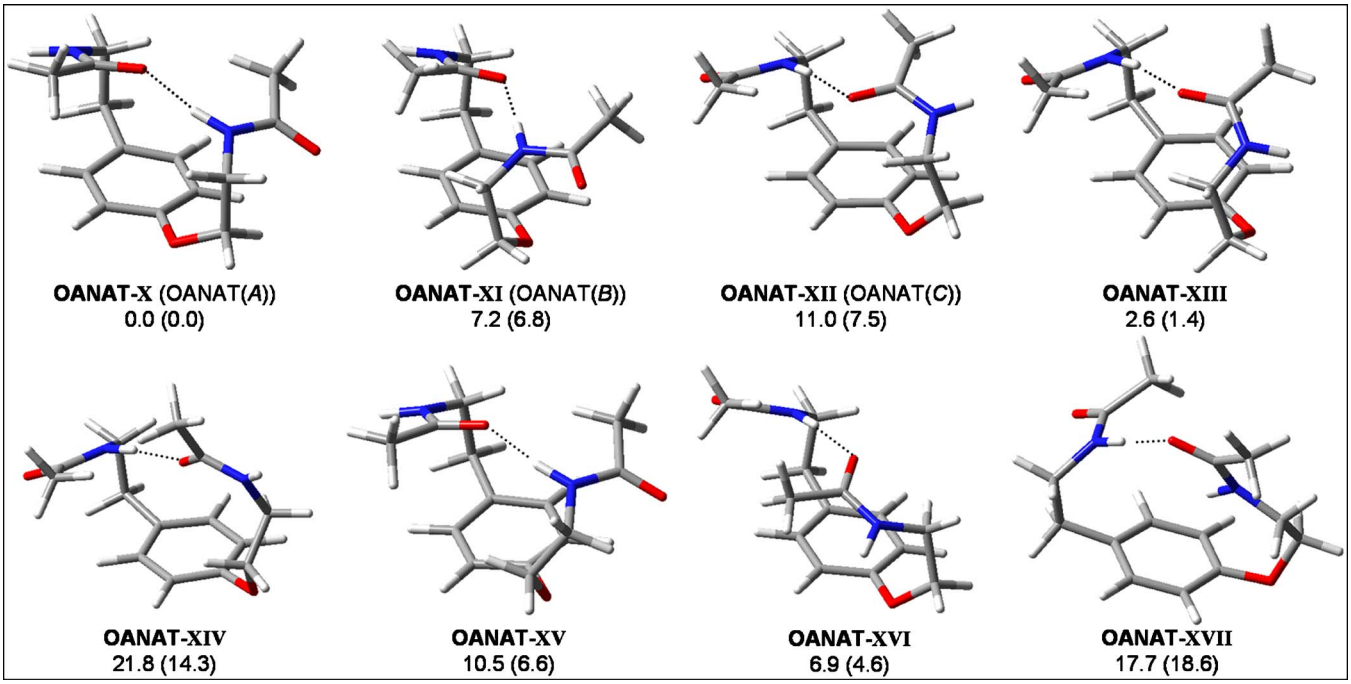

FIG. 15. (Color online) Conformers of OANAT that form interchain hydrogen bonds between amide groups. Optimized RIMP2/aug-cc-pVDZ′ energies (kJ/mol), vibrational zero point corrected with B3LYP frequencies, are given with relative free energies in parentheses. Note that OANAT-XVII is a *cis/trans* amide structure.

The assigned structures for NMPEA(*A*) and *B* shared the same gauche ethylacetamide chain conformation with different orientations of the methoxy group relative to it (gauche-*cis* and gauche-*trans*, Fig. 5). By analogy, we assign OANAT(*D*) and *E* to structures containing gauche alkyl side chain conformations that share the same alkoxy conformation but differ in the relative orientation of the two chains. Given the dominance of the *AGg* conformation of the alkoxy chain in NPOEA (20 times larger than others), it seems likely that the alkoxy chain in OANAT(*D*) and *E* assumes this conformation. Furthermore, the *AGg* conformation extends the alkoxy chain away from the aromatic ring, consistent with assigning the observed vibronic structure primarily to motions of the gauche alkyl chain. In NMPEA, the gauche-*trans* conformation has an S_0-S_1 origin red of gauche-*cis*. Thus OANAT(*D*) is tentatively assigned to the gauche-*trans*-*AGg* conformations (OANAT-III and/or OANAT-IV) and *E* to the gauche-*cis*-*AGg* conformations (OANAT-I and/or OANAT-II).

Using similar reasoning, conformer *F* of OANAT is tentatively assigned to one of the anti alkyl chain structures (OANAT V–VIII) shown in the bottom row of Fig. 14. The shift to the blue in OANAT(*F*) is reminiscent of conformer *C* of NMPEA, with its anti alkyl conformation, which is shifted by +52/43 cm^{-1} from NMPEA(*A*/*B*). The lack of vibronic activity indicates a weak interaction of the aromatic ring with both chains, in accordance with this assignment.

The RIDIR spectra of conformers *D*–*F* of OANAT serve as a powerful diagnostic for strengthening these assignments. One might anticipate that the amide NH stretch frequencies associated with the noninteracting side chain conformations of OANAT would be very close to those found in the analogous conformers of NPOEA and NPEA (or NMPEA). In that case it should be possible to predict the NH stretch frequencies based on our tentative assignments. In OANAT(*D*) and *E*, the gauche alkyl chain conformation should have NH stretch fundamentals near 3482 cm^{-1} [its value in NMPEA(*A*/*B*)], while the anti alkyl chain in OANAT(*F*) should be near 3495 cm^{-1} [based on NMPEA(*C*)]. This condition is precisely what is observed, with OANAT(*D*) and *E* possessing NH stretch transitions at 3483 cm^{-1} and OANAT(*F*) at 3495 cm^{-1}. Furthermore, if the *AGg* alkoxy chain conformation of NPOEA is present in all three independent-chain conformations of OANAT, all three spectra should exhibit a second amide NH stretch fundamental near 3491 cm^{-1}. Again this condition is observed, with transitions at 3491, 3493, and 3490 cm^{-1} in OANAT(*D*–*F*), respectively.

The tentative assignments for OANAT(*D*–*F*) are incomplete in the sense that they have not distinguished between structures that have the same alkyl/alkoxy chain conformations in different orientations relative to one another. Thus, there are two possibilities for OANAT(*D*) (III or IV), two for OANAT(*E*) (I or II), and four for OANAT(*F*) (V–VIII). According to the calculations, there is little energetic preference to separate these possibilities. This observation necessitates asking why all eight possibilities are not observed. There are three possible answers. First, if the barriers separating some of the conformers are small, cooling in the expansion could efficiently remove population from the higher energy to the lower energy forms in each group. Second, transitions due to the individual structures could be overlapped in the ultraviolet if the shifts induced by different relative orientations of the two chains were too small to be resolved. Third, the transitions due to other conformers could be present and resolved, but have not been clearly identified in the congested

spectra that characterize this blue region of the R2PI spectrum. This latter circumstance seems to be at play for OANAT(*F*). The R2PI spectrum of OANAT (Figs. 11 and 12, top right) shows several closely spaced transitions just to the blue of *F* which do not burn with *F* or any of the other conformers of OANAT. We were not successful in carrying out UV-UV hole-burning spectroscopy on these transitions. However, their presence as unaccounted for transitions in this region suggests that more than one of the anti-AG_g conformers from OANAT-V–VIII may contribute to the spectrum in this region.

F. Interchain H-bonded conformations

Conformers *A* and *B* of OANAT display long Franck-Condon progressions in their hole-burn spectra [Figs. 12(b) and 12(c)]. This observation is not surprising given that the process of forming an interchain hydrogen bond must necessarily bring the two side chains together over the ring, leading to a strong interaction between the chains and the aromatic ring.

The interacting side-chain conformations can be broken into two classes of conformations: alkyl chain donating and alkoxy chain donating, where donating refers to the amide nitrogen donating its hydrogen to the opposite chain's carbonyl oxygen to form a hydrogen bond. In forming these interchain H bonds, the conformational preferences of the individual chains have been compromised in order to form the H bond. Following careful searches, several interchain H-bonded structures were identified, among them OANAT-X–XVII (Fig. 15). Of the *trans/trans* amide structures investigated, OANAT-X, XI, and XV are alkoxy chain donating structures, while OANAT-XII, XIII, XIV, and XVI are alkyl chain donating structures. OANAT-X and XI have similar structures, differing in the orientation of the alkoxy chain, particularly the C_β–C_γ linkage, relative to the alkyl chain. The same observation holds true for OANAT-XII and XIII. OANAT-XIV contains an alkoxy chain that is more vertical and allows for a more nearly linear NH···OC hydrogen bond.

An analysis of S_0-S_1 origin transition frequencies serves as a starting point for our assignments. TDDFT and RICC2 calculations predict that the alkoxy chain donating structures X and XI should have large redshifts of up to -1500 cm^{-1} (Table I) from OANAT-I, while the alkyl chain donating structures (XII–XIV and XVI) have much smaller shifts, hundreds of wavenumbers both blue and red. On this basis, we assign OANAT(*A*) and OANAT(*B*) as alkoxy-donating structures and OANAT(*C*) to an alkyl-donating structure. OANAT-X can be viewed as gauche-*trans* and OANAT-XI as gauche-*cis*. Thus, by analogy to NMPEA, OANAT(*A*) is tentatively assigned as OANAT-X and OANAT(*B*) as OANAT-XI.[102]

The position of the S_0-S_1 origin of OANAT(*C*) provides a first point of distinction among the four possible alkyl-donating structures OANAT XII–XIV and XVI. The origin of OANAT(*C*) is in the same region as OANAT(*D*) and OANAT(*E*), but redshifted about 60 cm^{-1}. TDDFT and RICC2 calculations predict the S_0-S_1 origins for OANAT-XII, XIV, and XVI to be to the blue of OANAT-I and that of OANAT-XIII to be to the red of OANAT-I. These results argue for an assignment of OANAT(*C*) to OANAT-XIII.

The RIDIR spectra provide further input to these assignments. In the H-bonded NH stretch region, OANAT(*C*) has a NH stretch fundamental (3386 cm^{-1}) slightly shifted down in frequency from the alkoxy-donating pair (3390 cm^{-1}). The H-bonded NH stretch fundamentals for OANAT XII–XIV and XVI are predicted by B3LYP calculations to occur at 3382, 3411, 3447, and 3419 cm^{-1}, respectively, compared to 3411, 3399, and 3428 cm^{-1} for the alkoxy-donating structures OANAT-X, XI, and XV. Thus, only OANAT-XII has a calculated H-bonded NH stretch frequency below that of OANAT-X and XI, as is observed.

Experimentally, the free amide NH stretch fundamentals of OANAT(*A*) and OANAT(*B*) occur at 3479 cm^{-1}, a value close to that found in the gauche alkyl chain of NMPEA (3482 cm^{-1}). By comparison, the corresponding transition in OANAT(*C*) (3475 cm^{-1}) is a few wavenumbers lower. In keeping with this, the calculated scaled harmonic DFT B3LYP frequencies for the alkoxy-donating structures OANAT-X and XI (3479 and 3480 cm^{-1}) are slightly higher in frequency than that for the alkyl-donating structures OANAT-XII, XIII, and XVI (all at 3477 cm^{-1}). At the same time, the calculations predict a significantly higher frequency (3487 cm^{-1}) for OANAT-XIV, arguing for an assignment of OANAT-C to OANAT-XII, XII, or XVI. However, due to the failure of the B3LYP calculations to quantitatively predict NH stretch frequency shifts close to those observed for NMPEA and NPOEA, these assignments remain tentative. Thus, taken as a whole, the available data and computational results argue against an assignment of OANAT(*C*) to OANAT-XIV or XVI, but do not permit us to decide between OANAT-XII and XIII.

VI. DISCUSSION

The combined experimental and theoretical results presented in Sec. V have established single-conformation infrared and ultraviolet spectral signatures and provided a consistent set of conformational assignments for NPEA, NPOEA, NMPEA, and OANAT. NPEA and NPOEA are single-chain ethylacetamide and ethoxyacetamide phenyl derivatives, while NMPEA and OANAT are double chains. By comparing the single-chain and double-chain results, we hope to understand how the conformational preferences of the single-chain analogs are reflected in the observed double-chain conformers, or modified by interactions between the two chains.

A. The single-chain conformational preferences

The jet-cooled R2PI spectrum of NPEA is dominated by a single conformer with an out-of-plane orientation for the ethylacetamide chain that places the amide group in a gauche position relative to the ring, stabilized by the interaction of the amide NH with the phenyl ring. Four conformers of NPOEA were detected and characterized. The dominant transitions in the UV spectrum, appearing with intensities 20 times larger than any others, are assigned to a single AG_g conformation (NPOEA-I in Fig. 8) of the alkoxy chain in

which the $O-CH_2$ group is in plane in order to facilitate hyperconjugation of the oxygen lone pairs with the ring. The minor conformers vary in the degree to which they fold back over the ring.

NMPEA adds a methoxy group to NPEA in the *para* position on the phenyl ring. As such, it is the simplest alkyl/alkoxy double chain that probes the primary effects of the first two atoms in the alkoxy chain of OANAT. Three conformations of NMPEA were observed, two with nearly identical spectra assigned to the same gauche NPEA ethylacetamide conformation differing in the orientation of the chain relative to the methoxy group. A third minor conformer of NMPEA is assigned to an anti ethylacetamide chain conformation, indicating that the presence of the methoxy group on the ring enhances population in the anti alkyl chain conformation relative to gauche.

Having made these assignments, it is appropriate to return to the disconnectivity diagrams for NMPEA and NPOEA shown in Figs. 1(a) and 1(b) to assess their relationship to the experimental findings. A total of 18 NMPEA minima were found with GAFF, nine *cis*-amide and nine *trans*-amide. The pairs of minima associated with I–III differ only in the orientation of the terminal methyl group, and these distinct methyl structures from GAFF collapse to a single minimum under B3LYP or RIMP2 optimization, reducing the number of true minima in NMPEA from 18 to 15. The three observed conformers ($A-C$) are assigned to structures II, I, and III, respectively, labeled in the diagram. These conformational minima are located by GAFF at the bottom of the *trans*-amide gauche and anti branches of the diagram. The force field also correctly places the gauche minima below anti, in keeping with higher level theory and the dominance of transitions due to I and II over III in the experimental spectra (Table I, Fig. 4).

In NPOEA, the GAFF calculations find nine low-energy *trans*-amide minima, which reduce to seven unique minima when reoptimized with the B3LYP or RIMP2 methods. As previously, the "extra" structures differ in the orientation of the terminal methyl hydrogens. The Roman numerals in Fig. 1(b) are attached to low-lying minima calculated with higher levels of theory (Fig. 8). The experimentally observed conformers ($A-D$) are assigned to low-lying minima on the GAFF disconnectivity diagram (I, IV, III, and V, respectively).

While the disconnectivity diagrams using the GAFF do correctly predict the isomerization barriers between *trans*- and *cis*-amide branches of the potential energy surface, not all barriers are correctly predicted. For example, the isomerization between NMPEA-II and III, consisting of a simple $\approx 90°$ rotation of the C_X-C_Y bond, is predicted by GAFF to be about 48 kJ/mol while RIMP2 calculations predict the barrier to be 25 kJ/mol. In the same way, the barrier for internal rotation of the methoxy group in NMPEA is predicted by GAFF to be 6 kJ/mol, compared to the experimentally observed value, 9.7 kJ/mol.[103]

B. Electronic frequency shifts in the alkoxy chains

One of the striking aspects of the ultraviolet spectroscopy of this series of molecules is the very large shifts in the wavelengths of S_0-S_1 origins associated with conformations of the alkoxy chain. The electronic frequency shifts of the conformers of NPOEA are spread over 760 cm^{-1}, while those in OANAT span over 1000 cm^{-1}. By comparison, the various conformations of NMPEA have S_0-S_1 origins within 52 cm^{-1} of one another, nearly a factor of 20 less. This sensitivity of the S_0-S_1 energy separation to the conformation of the ethoxyacetamide chain is also predicted by both TDDFT and RICC2 calculations, serving as a distinguishing feature that guided the conformational assignments.

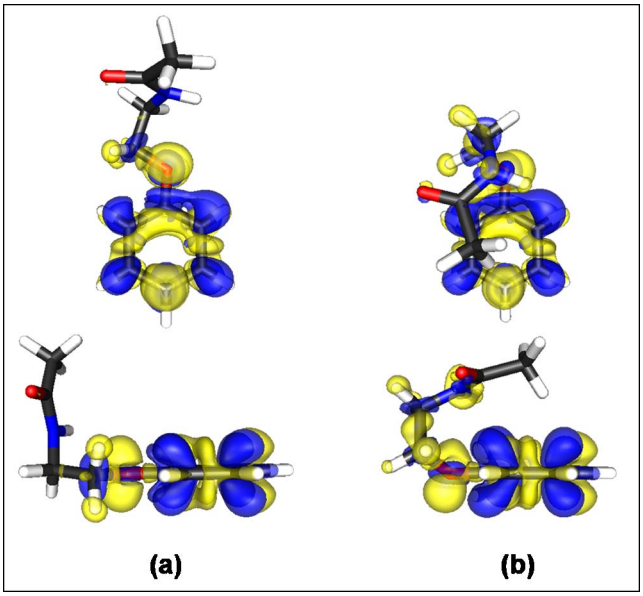

FIG. 16. (Color online) Electron density differences for the S_0-S_1 transitions of (a) NPOEA-I and (b) NPOEA-V[b], calculated at the RICC2 level of theory. Dark (light) indicates areas of increased (decreased) electron density upon electronic excitation.

Based on the assignments presented above, origin transitions with the largest S_0-S_1 separations are associated with extended structures while those with the smallest S_0-S_1 separations are associated with folded structures of the alkoxy chain. The large difference between the S_0-S_1 separations of extended and folded conformers can be understood in terms of the shifts in the energies of the frontier orbitals. For example, we note that the gap between the highest occupied molecular orbital (HOMO) and the lowest unoccupied molecular orbital (LUMO) [from B3LYP calculations with the 6-311+G(d) basis set] of the folded conformer OANAT-X is about 0.3 eV less than that of the extended conformer OANAT-I, with most of the shift due to destabilization of the HOMO in the folded structure. Examination of the electron density differences for S_0-S_1 transitions of the extended and folded conformers, NPOEA-I and NPOEA-V[b], shown in Fig. 16, reveals that this shift is a result of hyperconjugation between the $C_\beta-C_\gamma$ σ bond and the lone pair in the p-type orbital of the oxygen linkage.

C. Obtaining accurate relative energies for the conformers of OANAT

The disconnectivity diagram for the double-chain OANAT, shown in Fig. 1(c), was initially introduced simply as a means for visualizing the vastly increased complexity of

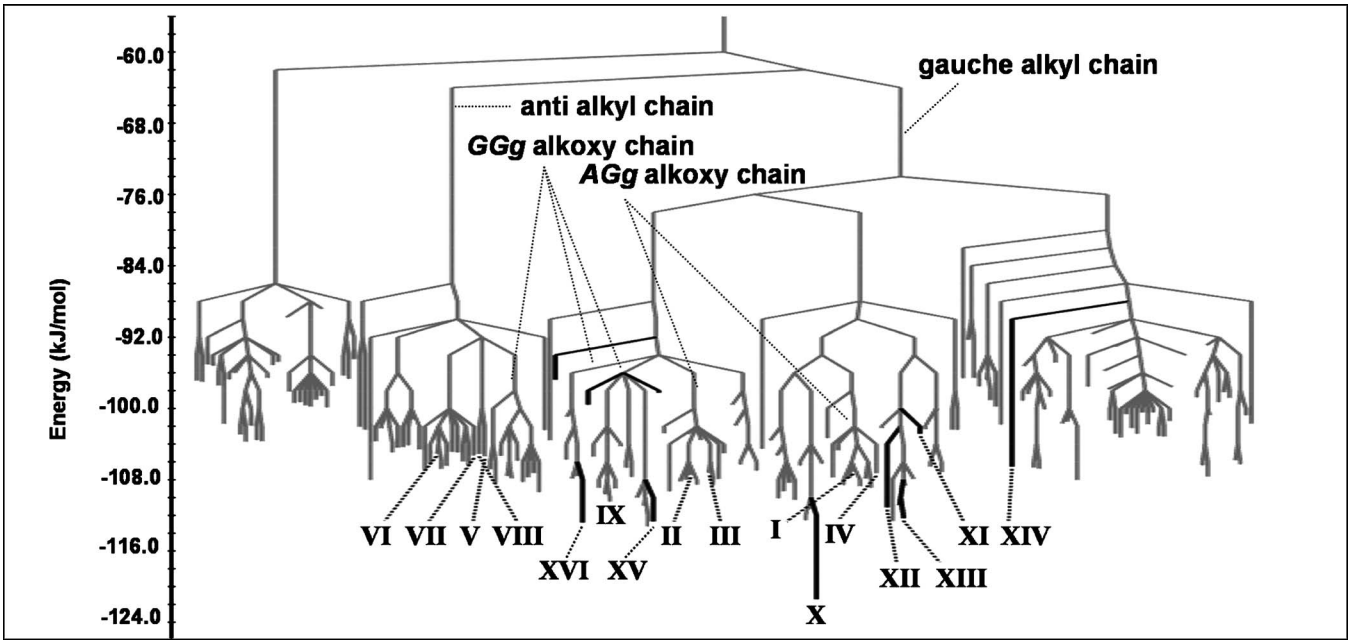

FIG. 17. Closeup view of the *trans/trans* amide portion of the OANAT disconnectivity diagram with major branches of structural families identified. Roman numerals label conformations on which higher level electronic structure calculations were performed. Lines colored black indicate conformers containing an interchain H bond.

its potential energy surface relative to the single-chain analogs NPEA, NMPEA, and NPOEA. Having carried out the single-conformation spectroscopy of OANAT, it is time to return to the disconnectivity diagram in order to assess the observations relative to the predictions of theory.

We have detected and assigned six conformational isomers of OANAT. Based primarily on the frequencies of the amide NH stretch fundamentals, we have classified all the observed conformers as *trans/trans* amides, with three being noninteracting chain conformers and three being interchain H-bonded conformers. Interestingly, the GAFF calculations [Fig. 1(c)] predict that seven *cis/trans* amide conformers are comparable in energy to the lowest-energy *trans/trans* amide conformers. These low-energy *cis/trans* structures are stabilized by interchain H bonds and through interaction of the NH group of the *cis* amide with the ring. When the most stable *cis/trans* amide (conformer XVII) found with GAFF is reoptimized using the RIMP2 method, it is found to be 16.9 kJ/mol higher in energy than the most stable *trans/trans* conformer. Moreover, vibrational zero-point and entropy corrections further destabilize the low-lying *cis/trans* isomers relative to the most stable *trans/trans* conformer. Thus it is not surprising that none of the *cis/trans* conformers of OANAT are observed in our experiments.

Figure 17 presents a closeup of the *trans/trans* amide region of the disconnectivity diagram of OANAT, calculated with the GAFF. As with the NMPEA and NPOEA diagrams [Figs. 1(a) and 1(b)], we have included Roman numeral labels for the OANAT structures characterized using electronic structure methods and shown in Figs. 14 and 15. The lines connecting transition states to minima that involve interchain H bonds are shown in black in order to distinguish them from the non-H-bonded minima. Our optimizations with GAFF identified a total of 195 *trans/trans* minima and 594 transition states. Since, as discussed above, about 20% of the local minima of NMPEA, NMPEA, and NPOEA located with GAFF reoptimized to other structures with the B3LYP and RIMP2 methods, we estimate that OANAT actually has about 125 *trans/trans* amide local minima, many of which are similar in energy and have structures based on low-lying single-chain conformations.

The conformational landscape of OANAT presents a significant challenge to theory on at least two fronts. First, subjecting all the minima and transition states discovered by GAFF to a systematic exploration at the RIMP2 level of theory would be computationally prohibitive. Deciding which structures to pursue and which to ignore is complicated by the fact that the experimental work has uncovered both interchain H-bonded and independent-chain structures. GAFF finds only six structures within 10 kJ/mol of the lowest-energy *trans/trans* isomer (structure X), but there are 126 conformations within the next 10 kJ/mol, most of which are non-H-bonded structures. In order to make the problem tractable, we have chosen a strategy that focuses attention on *trans/trans* amide (i) double-chain conformations built from the lowest-energy single-chain conformations (structures I–IX) and (ii) interchain H-bonded structures (X–XVI).

Second, these two broad classes of structures have properties that test the limits of present-day theory to obtain accurate structures and relative energies. Figure 18 summarizes the relative energies of the 17 benchmark structures of OANAT, calculated using the GAFF, B3LYP/6-311+G(*d*), B2PLYP/aug-cc-pVDZ′, and RIMP2/aug-cc-pVDZ′ theoretical methods. The B3LYP calculations predict that the independent-chain conformers are lower in energy than the interchain H-bonded conformers. However, all other theoretical approaches considered, including GAFF, predict that X, an interacting chain structure, is the lowest-energy conformer

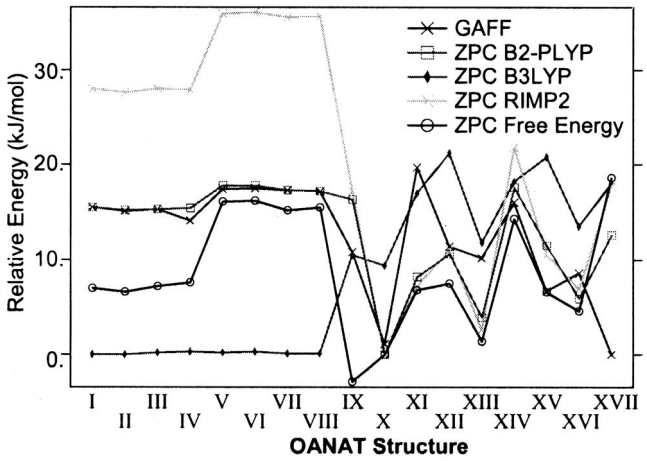

FIG. 18. Relative energies of the calculated structures of OANAT employing the indicated theoretical methods. Gibbs free energy corrections were calculated using B3LYP frequencies and RIMP2 energies.

of the 17 presented. Furthermore, the independent-chain conformers are predicted to be some 15–40 kJ/mol higher in energy with the GAFF, B2PLYP (which includes dispersion corrections to the BLYP density functional method),[104] and RIMP2 methods.

It is now well documented that standard density functional methods do not give accurate relative energies of different isomers of molecules in which intramolecular dispersion varies appreciably between isomers.[98,99] The MP2 and RIMP2 methods generally fare much better at predicting relative energies but can "overshoot" as has been found for benzene dimer[95] and for NPOEA, discussed above. Moreover, when dealing with the relative energies of compact and extended structures, basis set superposition error can be important for the size of basis sets used in this study. For example, single-point RIMP2 calculations with the aug-cc-pVTZ basis set using the RIMP2/aug-cc-pVDZ′ optimized geometries reduce the energy separation between NPOEA-I and NPOEA-V from 8 kJ/mol (aug-cc-pVDZ′ result) to 2.5 kJ/mol. This energy difference could be further reduced or perhaps even reversed upon adoption of still larger basis sets. Reoptimization of the geometries at the RIMP2 level using a larger basis set than employed here could also introduce significant changes in the relative energies. Ideally, one would include high order correlation effects using the CCSD(T) method together with large basis sets, but such calculations would be computationally prohibitive. The B2PLYP method of Grimme combines the BLYP functional with both RIMP2 and additional long-range corrections for dispersion.[104] For some systems this approach has been found to give relative energies superior to those from MP2 calculations.[105]

D. Entropy-driven population distributions in OANAT

The clear prediction of theory displayed in Fig. 18 is that the independent-chain conformers of OANAT (I–IX) are much higher in energy than the most stable H-bonded conformers. Despite this, we observe three independent-chain conformers, with spectral intensities that are comparable to their H-bonded counterparts.

In much of the previous work on the spectroscopy of conformationally flexible molecules, the comparison between experiment and theory was carried out by first locating the global minimum structure and then screening other conformers by comparison of their relative energies to that of the global minimum. In the limit that collisional cooling is fast compared to isomerization, the populations observed downstream in the expansion preserve the preexpansion populations dictated by the Boltzmann distribution at the nozzle temperature (450 K in this case). These populations are often estimated based on the relative energies of the zero-point levels, extracted from the calculations. By this measure, none of the independent-chain structures should be observed. Based on the relative energies from Fig. 18, the population of any of the independent-chain conformers is a tiny fraction of structure X, ranging from 2% (GAFF), 1% (B2PLYP), and 0.03% (RIMP2). In the limit that the barriers to isomerization are sufficiently low, population will be funneled out of the higher-energy conformers toward those with lower energy, reducing the population of the independent-chain conformers still further.

The solution is one recognized in several previous studies;[13–23] namely, that the equilibrium, preexpansion populations are dictated, not by ΔE (the difference in internal energies) but by ΔG (the difference in free energies). In most cases studied to date, the differences between ΔG and ΔE are modest: all conformers have similar flexibility, with similar low-frequency torsional vibrations that lead to similar energy-dependent densities of vibrational states and entropies. However, the two classes of structures present in OANAT provide a dramatic example where free energy corrections are essential to even a qualitatively correct understanding of the experimental results.

The interchain H-bonded conformers are energetically stable, but the two chains are highly restricted in forming the interchain H bond. The two chains need to fold back over the ring in order to position the two amide groups in close proximity for H-bond formation, thereby lowering the entropy of these structures. On the other hand, the independent-chain conformers have two flexible side chains that undergo torsions which are not restricted by interactions with the other chain. Thus, a large number of low-frequency torsional vibrations are produced that dominate the density of vibrational states, increasing the entropy and lowering the free energy of these conformers.

Table I presents the relative free energy corrections and final free energy differences for the 17 benchmark conformers of OANAT, computed at 450 K using the RIMP2 energies and the B3LYP/6-311+G(d) harmonic vibrational frequencies. For NPEA, NMPEA, and NPOEA, for which we have both B3LYP and RIMP2 vibrational frequencies, it was found that the zero point energy and entropic corrections to the relative energies of the various isomers are approximately the same with the two sets of frequencies. The corrections are large for OANAT, with independent-chain conformers stabilized approximately 20 kJ/mol relative to the H-bonded conformers. For visualization of this effect, Fig. 18 includes the free energy differences between the conformers using the RIMP2 relative energies. We see that the free

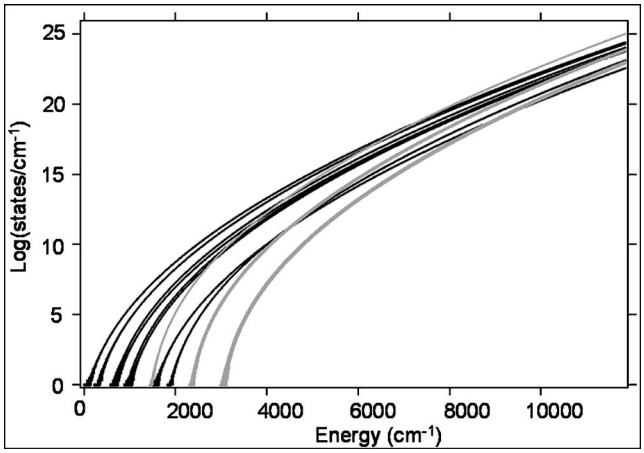

FIG. 19. Log of the density of states vs energy for the indicated conformers of OANAT. Black and grey traces are for interacting chain and independent-chain structures, respectively. The energy axis intercept for each trace is the relative zero point corrected RIMP2 energy.

energies of the H-bonded and non-H-bonded conformers are now comparable to one another, consistent with the observation of both kinds of isomers in the experimental study.

The fact that entropic effects can overcome the significant enthalpy differences between the H-bonded and non-H-bonded conformers arises because of the much steeper increase in density of states of the floppy independent-chain conformers relative to the restricted H-bonded ones, as is illustrated in Fig. 19. The calculated vibrational density of states of the two types of conformers crosses at about 108 kJ/mol, similar to the average internal vibrational energy (100 kJ/mol) available to the conformers at 450 K. A second effect that may contribute to the enhancement of population in the independent-chain conformers relative to H-bonded ones is that there are many more of the former relative to the latter, as can be seen from Fig. 17.

This brings us full circle back to a question that arose immediately upon completion of the disconnectivity diagrams for OANAT [Figs. 1(c) and 17]: If there are so many similar-energy independent-chain conformers, why do we see only three after cooling in the expansion? One answer is that some of the complexity may be hidden in the congestion of the ultraviolet spectrum (Figs. 11 and 12) that prevents us from resolving others that are present. However, it also seems likely that cooling in the expansion may gather population from several similar independent-chain conformers into the lowest-energy conformer in a given subspace of the potential energy surface, contributing to the enhancement of the population of a single conformer representing that subspace. The disconnectivity diagram does show divisions into such subspaces, and, in fact, several of the conformers I–IX are at or near the bottom of different branches that are separated by comparatively small barriers.

VII. CONCLUSIONS

The present study has provided a dramatic example of the effects of entropy on the observed populations of a tailor-made, double-chain flexible molecule. Arguments based on internal energy differences alone would have caused us to categorically dismiss all independent-chain conformers. However, three such conformers are observed with populations comparable to those of the lower-energy H-bonded conformers.

The principal molecule studied, OANAT, also turns out to be an ideal system for testing model potentials and electronic structure methods. There are conformers in which the two chains are essentially noninteracting as well as those in which the two chains are H bonded, which necessarily also enhances interactions between the side chains and the aromatic ring. The B3LYP method is found to be inadequate for predicting the relative energies of the two types of isomers, primarily because of its failure to account for long-range dispersion interactions.[98,99] Although GAFF, RIMP2, and B2LYP (which includes dispersion corrections) all predict the folded structures to be favored (focusing on electronic energies), there are significant differences between the results of these three methods. Ultimately, in order to resolve the observation of independent-chain structures of OANAT with the predictions that such structures should be more than 20 kJ/mol less stable than H-bonded structures, the conformational free energies were calculated using the preexpansion temperature. We found that the preexpansion relative free energies were comparable for both classes of molecules. This finding, when combined with the extent to which independent chains outnumber the H-bonded chain structures, offers an explanation for the experimental observation of both types of structures: entropy-driven population distributions.

ACKNOWLEDGMENTS

V.A.S., E.E.B., J.R.C., W.H.J., and T.S.Z. acknowledge support from the National Science Foundation (CHE-0551075) for this research. D.P.S. acknowledges the New Zealand Foundation for Research, Science and Technology for a postdoctoral fellowship. K.D.J. acknowledges support from the NSF (CHE-0518253).

[1] A. Abo-Riziq, B. O. Crews, M. P. Callahan, L. Grace, and M. S. de Vries, Angew. Chem. **118**, 5290 (2006).
[2] R. Brause, H. Fricke, M. Gerhards, R. Weinkauf, and K. Kleinermanns, Chem. Phys. **327**, 43 (2006).
[3] W. Chin, J. P. Dognon, C. Canuel, F. Piuzzi, I. Dimicoli, M. Mons, I. Compagnon, G. von Helden, and G. Meijer, J. Chem. Phys. **122**, 054317 (2005).
[4] W. Chin, F. Piuzzi, I. Dimicoli, and M. Mons, Phys. Chem. Chem. Phys. **8**, 1033 (2006).
[5] T. Ebata, T. Hashimoto, T. Ito, Y. Inokuchi, F. Altunsu, B. Brutschy, and P. Tarakeshwar, Phys. Chem. Chem. Phys. **8**, 4783 (2006).
[6] H. Fricke, A. Gerlach, C. Unterberg, P. Rzepecki, T. Schrader, and M. Gerhards, Phys. Chem. Chem. Phys. **6**, 4636 (2004).
[7] N. A. Macleod and J. P. Simons, Phys. Chem. Chem. Phys. **6**, 2878 (2004).
[8] M. Schmitt, R. Brause, C. M. Marian, S. Salzmann, and W. L. Meerts, J. Chem. Phys. **125**, 124309 (2006).
[9] M. Schmitt, K. Feng, M. Boehm, and K. Kleinermanns, J. Chem. Phys. **125**, 144303 (2006).
[10] J. T. Yi, E. G. Robertson, and D. W. Pratt, Phys. Chem. Chem. Phys. **4**, 5244 (2002).
[11] T. S. Zwier, J. Phys. Chem. A **110**, 4133 (2006).
[12] I. Unamuno, J. A. Fernández, A. Longarte, and F. Castaño, J. Phys. Chem. A **104**, 4364 (2000).
[13] S. Basu and J. L. Knee, J. Phys. Chem. A **105**, 5842 (2001).
[14] P. Felder and H. H. Gunthard, Chem. Phys. **71**, 9 (1982).
[15] G. T. Fraser, R. D. Suenram, and C. L. Lugez, J. Phys. Chem. A **105**,

9859 (2001).
[16] P. D. Godfrey, R. D. Brown, and F. M. Rodgers, J. Mol. Struct. **376**, 65 (1996).
[17] A. Kaczor, I. D. Reva, L. M. Proniewicz, and R. Fausto, J. Phys. Chem. A **110**, 2360 (2006).
[18] D. Kim and T. Baer, Chem. Phys. **256**, 251 (2000).
[19] M. R. S. Mccoustra, M. Hippler, and J. Pfab, Chem. Phys. Lett. **200**, 451 (1992).
[20] T. F. Miller, D. C. Clary, and A. J. H. M. Meijer, J. Chem. Phys. **122**, 244323 (2005).
[21] J. D. Pitts, J. L. Knee, and S. Wategaonkar, J. Chem. Phys. **110**, 3378 (1999).
[22] I. D. Reva, S. G. Stepanian, L. Adamowicz, and R. Fausto, Chem. Phys. Lett. **374**, 631 (2003).
[23] R. S. Ruoff, T. D. Klots, T. Emilsson, and H. S. Gutowsky, J. Chem. Phys. **93**, 3142 (1990).
[24] E. G. Robertson and J. P. Simons, Phys. Chem. Chem. Phys. **3**, 1 (2001).
[25] J. R. Clarkson, E. Baquero, V. A. Shubert, E. M. Myshakin, K. D. Jordan, and T. S. Zwier, Science **307**, 1443 (2005).
[26] J. R. Clarkson, E. Baquero, and T. S. Zwier, J. Chem. Phys. **122**, 214312 (2005).
[27] J. R. Clarkson, B. C. Dian, L. Moriggi, A. DeFusco, V. McCarthy, K. D. Jordan, and T. S. Zwier, J. Chem. Phys. **122**, 214311 (2005).
[28] B. C. Dian, J. R. Clarkson, and T. S. Zwier, Science **303**, 1169 (2004).
[29] T. M. Selby, J. R. Clarkson, D. Mitchell, J. A. J. Fitzpatrick, H. D. Lee, D. W. Pratt, and T. S. Zwier, J. Phys. Chem. A **109**, 4484 (2005).
[30] L. C. Snoek, E. G. Robertson, R. T. Krocmer, and J. P. Simons, Chem. Phys. Lett. **321**, 49 (2000).
[31] I. Compagnon, J. Oomens, G. Meijer, and G. von Helden, J. Am. Chem. Soc. **128**, 3592 (2006).
[32] W. Chin, M. Mons, F. Piuzzi, B. Tardivel, I. Dimicoli, L. Gorb, and J. Leszczynski, J. Phys. Chem. A **108**, 8237 (2004).
[33] H. Satzger, D. Townsend, M. Z. Zgierski, S. Patchkovskii, S. Ullrich, and A. Stolow, Proc. Natl. Acad. Sci. U.S.A. **103**, 10196 (2006).
[34] E. Samoylova, H. Lippert, S. Ullrich, I. V. Hertel, W. Radloff, and T. Schultz, J. Am. Chem. Soc. **127**, 1782 (2005).
[35] S. Ullrich, T. Schultz, M. Z. Zgierski, and A. Stolow, J. Am. Chem. Soc. **126**, 2262 (2004).
[36] S. Ullrich, T. Schultz, M. Z. Zgierski, and A. Stolow, Phys. Chem. Chem. Phys. **6**, 2796 (2004).
[37] C. Plutzer and K. Kleinermanns, Phys. Chem. Chem. Phys. **4**, 4877 (2002).
[38] E. Nir, C. Janzen, P. Imhof, K. Kleinermanns, and M. S. de Vries, J. Chem. Phys. **115**, 4604 (2001).
[39] F. Piuzzi, M. Mons, I. Dimicoli, B. Tardivel, and Q. Zhao, Chem. Phys. **270**, 205 (2001).
[40] N. J. Kim, G. Jeong, Y. S. Kim, J. Sung, S. K. Kim, and Y. D. Park, J. Chem. Phys. **113**, 10051 (2000).
[41] B. C. Dian, A. Longarte, S. Mercier, D. A. Evans, D. J. Wales, and T. S. Zwier, J. Chem. Phys. **117**, 10688 (2002).
[42] B. C. Dian, A. Longarte, and T. S. Zwier, Science **296**, 2369 (2002).
[43] W. Chin, M. Mons, J. P. Dognon, R. Mirasol, G. Chass, I. Dimicoli, F. Piuzzi, P. Butz, B. Tardivel, I. Compagnon, G. von Helden, and B. Meijer, J. Phys. Chem. A **109**, 5281 (2005).
[44] W. Chin, F. Piuzzi, J. P. Dognon, I. Dimicoli, and M. Mons, J. Chem. Phys. **123**, 084301 (2005).
[45] S. Wiedemann, A. Metsala, D. Nolting, and R. Weinkauf, Phys. Chem. Chem. Phys. **6**, 2641 (2004).
[46] I. Hunig and K. Kleinermanns, Phys. Chem. Chem. Phys. **6**, 2650 (2004).
[47] W. Chin, M. Mons, J. P. Dognon, F. Piuzzi, B. Tardivel, and I. Dimicoli, Phys. Chem. Chem. Phys. **6**, 2700 (2004).
[48] C. Unterberg, A. Gerlach, T. Schrader, and M. Gerhards, J. Chem. Phys. **118**, 8296 (2003).
[49] I. Hunig, K. A. Seefeld, and K. Kleinermanns, Chem. Phys. Lett. **369**, 173 (2003).
[50] B. C. Dian, A. Longarte, and T. S. Zwier, Science **296**, 2396 (2002).
[51] O. M. Becker and M. Karplus, J. Chem. Phys. **106**, 1495 (1997).
[52] J. Wang, R. M. Wolf, J. W. Caldwell, P. A. Kollman, and D. A. Case, J. Comput. Chem. **25**, 1157 (2004).
[53] P. S. Li, X. G. Chen, E. Shulin, and S. A. Asher, J. Am. Chem. Soc. **119**, 1116 (1997).
[54] G. Scherer, M. L. Kramer, M. Schutkowski, U. Reimer, and G. Fischer, J. Am. Chem. Soc. **120**, 5568 (1998).
[55] C. Schiene-Fischer and G. Fischer, J. Am. Chem. Soc. **123**, 6227 (2001).
[56] See EPAPS Document No. E-JCPSA6-127-010743 for all supplementary information, including syntheses, NPEA optimized structures, and RIDIR and SVLF spectra of NMPEA and NPOEA. This document can be reached through a direct link in the online article's HTML reference section or via the EPAPS homepage (http://www.aip.org/pubservs/epaps.html).
[57] R. H. Page, Y. R. Shen, and Y. T. Lee, J. Chem. Phys. **88**, 4621 (1988).
[58] T. S. Zwier, Annu. Rev. Phys. Chem. **47**, 205 (1996).
[59] J. A. Stearns, A. Das, and T. S. Zwier, Phys. Chem. Chem. Phys. **6**, 2605 (2004).
[60] P. J. Breen, E. R. Bernstein, and J. I. Seeman, J. Chem. Phys. **87**, 3269 (1987).
[61] E. R. Bernstein, H.-S. Im, M. A. Young, H. V. Secor, R. L. Bassfield, and J. I. Seeman, J. Org. Chem. **56**, 6059 (1991).
[62] J. A. Dickinson, M. R. Hockridge, R. T. Kroemer, E. G. Robertson, J. P. Simons, J. McCombie, and M. Walker, J. Am. Chem. Soc. **120**, 2622 (1998).
[63] S. J. Martinez III, J. C. Alfano, and D. H. Levy, J. Mol. Spectrosc. **158**, 82 (1993).
[64] S. Sun and E. R. Bernstein, J. Am. Chem. Soc. **118**, 5086 (1996).
[65] G. L. Grunewald and M. W. Creese, J. Comput. Chem. **9**, 315 (1986).
[66] J. A. Fernández, I. Unamuno, and F. Castaño, J. Phys. Chem. A **105**, 9993 (2001).
[67] E. G. Robertson, J. P. Simons, and M. Mons, J. Phys. Chem. A **105**, 9990 (2001).
[68] J. R. Carney and T. S. Zwier, J. Phys. Chem. A **104**, 8677 (2000).
[69] J. R. Carney and T. S. Zwier, Chem. Phys. Lett. **341**, 77 (2001).
[70] L. A. Philips, S. P. Webb, S. J. Martinez, G. R. Fleming, and D. H. Levy, J. Am. Chem. Soc. **110**, 1352 (1988).
[71] P. J. Breen, E. R. Bernstein, H. V. Secor, and J. I. Seeman, J. Am. Chem. Soc. **111**, 1958 (1989).
[72] C. T. Lee, W. T. Yang, and R. G. Parr, Phys. Rev. B **37**, 785 (1988).
[73] A. D. Becke, J. Chem. Phys. **98**, 5648 (1993).
[74] M. Feyereisen, G. Fitzgerald, and A. Komornicki, Chem. Phys. Lett. **208**, 359 (1993).
[75] O. Vahtras, J. Almlof, and M. W. Feyereisen, Chem. Phys. Lett. **213**, 514 (1993).
[76] D. E. Bernholdt and R. J. Harrison, Chem. Phys. Lett. **250**, 477 (1996).
[77] D. J. Wales and J. P. K. Doye, J. Phys. Chem. A **101**, 5111 (1997).
[78] D. C. Liu and J. Nocedal, Math. Program. **45**, 503 (1989).
[79] http://www-wales.ch.cam.ac.uk/software.html
[80] C. J. Cerjan and W. H. Miller, J. Chem. Phys. **75**, 2800 (1981).
[81] D. J. Wales and T. R. Walsh, J. Chem. Phys. **105**, 6957 (1996).
[82] M. J. Frisch, J. A. Pople, and J. S. Binkley, J. Chem. Phys. **80**, 3265 (1984).
[83] D. E. Woon and T. H. Dunning, J. Chem. Phys. **103**, 4572 (1995).
[84] T. H. Dunning, J. Chem. Phys. **90**, 1007 (1989).
[85] R. A. Kendall, T. H. Dunning, and R. J. Harrison, J. Chem. Phys. **96**, 6796 (1992).
[86] D. E. Woon and T. H. Dunning, J. Chem. Phys. **100**, 2975 (1994).
[87] D. E. Woon and T. H. Dunning, J. Chem. Phys. **98**, 1358 (1993).
[88] K. A. Peterson and T. H. Dunning, J. Chem. Phys. **117**, 10548 (2002).
[89] C. Hättig and F. Weigend, J. Chem. Phys. **113**, 5154 (2000).
[90] M. J. Frisch, G. W. Trucks, H. B. Schlegel *et al.*, GAUSSIAN 03, Revision C.02, Gaussian, Inc., Wallingford, CT, 2004.
[91] R. Ahlrichs, M. Bar, M. Haser, H. Horn, and C. Kolmel, Chem. Phys. Lett. **162**, 165 (1989).
[92] J. B. Hopkins, D. E. Powers, S. Mukamel, and R. E. Smalley, J. Chem. Phys. **72**, 5049 (1980).
[93] J. B. Hopkins, D. E. Powers, and R. E. Smalley, J. Chem. Phys. **72**, 5039 (1980).
[94] The corresponding RIMP2 frequencies are 23 and 51 cm^{-1} for NPEA-I and 33 and 38 cm^{-1} for NPEA-II. Although the B3LYP torsional frequencies are a closer match to the experimental frequencies, it does not prove that the B3LYP method is superior in this case. The significant differences in the frequencies of the torsional modes predicted by the two methods can be partially attributed to the somewhat different geometries obtained, since RIMP2 seems to overestimate dispersive interactions while B3LYP does not properly account for them.
[95] J. G. Hill, J. A. Platts, and H.-J. Werner, Phys. Chem. Chem. Phys. **8**, 4072 (2006).
[96] C. Hampel, K. A. Peterson, and H. J. Werner, Chem. Phys. Lett. **190**, 1 (1992).

[97] K. Raghavachari, G. W. Trucks, J. A. Pople, and M. Headgordon, Chem. Phys. Lett. **157**, 479 (1989).
[98] M. D. Wodrich, C. Corminboeuf, and P. V. Schleyer, Org. Lett. **8**, 3631 (2006).
[99] Y. Zhao and D. G. Truhlar, J. Chem. Theory Comput. **3**, 289 (2007).
[100] The RIDIR scans for the minor conformers $B-D$ suffered from an interfering, IR-induced gain signal from conformer A when its infrared absorptions were encountered. This interference was due to warm NPOEA(A) produced when the IR laser was resonant with this dominant conformer. To overcome this interference, it was necessary to obtain RIDIR spectra for the minor conformers with the UV probe both on and off resonance with the conformer of interest. The UV off-resonance scans were taken by moving the UV probe approximately 5 cm^{-1} to the red of the on-resonance transition. Figure 6(b) presents the difference between on- and off-resonance spectra, thereby removing this interference.
[101] G. M. Florio, R. A. Christie, K. D. Jordan, and T. S. Zwier, J. Am. Chem. Soc. **124**, 10236 (2002).
[102] The tentative nature of the assignments of OANAT(A) and B arises because the calculations predict a significant difference in electronic frequency shifts and low-frequency torsional vibrational frequencies in OANAT-X and XI. Both these predictions are at odds with experiment, since OANAT(A) and B have S_0-S_1 origins within 3 cm^{-1} of one another, and nearly identical vibronic structure. This suggests that a more subtle geometry difference is responsible for the OANAT-(A/B) pair than is present in OANAT-X and XI.
[103] V. A. Shubert, C. Müller, E. E. Baquero, and T. S. Zwier (unpublished).
[104] S. Grimme, J. Chem. Phys. **124**, 034108 (2006).
[105] S. Grimme, J. Athony, T. Schwabe, and C. Muck-Lichtenfeld, Org. Biomol. Chem. **5**, 741 (2007).